Smoothed Particle Hydrodynamics method from a Large Eddy Simulation perspective

A. Di Mascio,[1] M. Antuono,[2] A. Colagrossi,[2, 3] and S. Marrone[2, 3]

[1] *CNR-IAC*

Istituto per le Applicazioni del Calcolo "Mauro Picone", Rome, Italy[a]

[2] *CNR-INSEAN*

Marine Technology Research Institute, Rome, Italy[b]

[3] *ECN / CNRS*

École Centrale Nantes, LHEEA Lab. , Nantes, France[c]

(Dated: 22 March 2017)

The Smoothed Particle Hydrodynamics (SPH) method, often used for the modelling of the Navier–Stokes equations by a meshless Lagrangian approach, is revisited from the point of view of Large Eddy Simulation (LES). To this aim, the LES filtering procedure is recast in a Lagrangian framework by defining a filter that moves with the positions of the fluid particles at the filtered velocity. It is shown that the SPH smoothing procedure can be reinterpreted as a sort of LES Lagrangian filtering, and that, besides the terms coming from the LES convolution, additional contributions (never accounted for in the SPH literature) appear in the equations when formulated in a filtered fashion. Appropriate closure formulas are derived for the additional terms and a preliminary numerical test is provided to show the main features of the proposed LES-SPH model.

---

[a] Electronic mail: a.dimascio@iac.cnr.it

[b] Electronic mail: matteo.antuono@cnr.it

[c] Electronic mail: andrea.colagrossi@cnr.it

INTRODUCTION

In the last decade, an increasing interest on Lagrangian particle methods has been growing on, mainly due to the possibility of modelling physical phenomena characterized by strong dynamics and large interface deformations. Among them, the Smoothed Particle Hydrodynamics (SPH) is enjoying a great success because of its conservation properties (it is relatively easy to write methods that conserve mass and energy), because of the almost absent numerical dissipation connected with convection, and because of its ability to handle free-surface flows with front evolution and fragmentations (see, for instance, Colagrossi and Landrini[1]).

Recently, a considerable effort has been addressed to solve the Navier–Stokes equations in Lagrangian formulation by SPH approaches (see, for instance, the reviews by Monaghan[2], Springel[3]), this being motivated by practical applications and by the desire of extending the scheme beyond its original framework. Unfortunately, the solution of the Navier-Stokes equations through SPH still represents a challenging problem, mainly due to the lack of sound theoretical works about turbulence modelling in the Lagrangian context. In fact, the Direct Numerical Simulation (DNS) of high Reynolds number flows remains infeasible because of the wide range of scales to be resolved, that span from the macroscopic ones (determined by the length and velocity scales characterizing the problem at hand) to the smallest dissipation scales (determined by the physical properties of the fluid).

An alternative approach is the solution of the Navier-Stokes equations in the time- or ensemble-averaging formulation given by Reynolds averaged Navier–Stokes (RANS) equations, where all the space and time turbulent scales are modelled. As large eddy evolution strongly depends on the boundary conditions and on the size of the domain, universal modelling for RANS is extremely difficult (see, for instance, Wilcox[4]). In SPH, several attempts to use RANS approaches exist, these all relying on a direct inclusion of $\kappa-\epsilon$ models (see, for example, Violeau and Issa[5], De Padova et al.[6], Leroy et al.[7]).

The approach that lies in the middle between DNS and RANS is the Large Eddy Simulation (LES), where only sub–grid turbulent eddies are modelled by space filtering, whereas the largest eddies are directly simulated (see, for instance, the classical reviews by Lesieur and Métais[8], Piomelli[9], Meneveau and Katz[10], Piomelli and Balaras[11]). LES modelling is expected to be easier than RANS modelling, because, when the discretization

is fine enough, the small sub–grid eddies should be closer to an "isotropic and homogeneous" scenario and therefore much less dependent on the specific problem under investigation. This (and the increased computer power) is probably the reason that determined the success of LES approaches in the last years, possibly in conjunction with zonal approaches, like Detached Eddy Simulation (see the review in Spalart[12]), that bypass the strict requirements for boundary layer simulations. In addition to these considerations, there is a further crucial aspect that makes the LES approach most suited for modelling the Navier-Stokes equations in the SPH scaffold, i.e. the structure of the SPH itself. Here the differential operators are approximated by a space filtering approach that somehow recalls the space filtering used in LES modelling, although based on a totally different starting point and with a different goal. In SPH, in fact, the building block is the substitution of the differential operators of the Navier–Stokes equations by their smoothed counterpart (see, for example, Colagrossi et al.[13,14]). This may be regarded as a convolution of each single operator with a "mollified" Dirac function centred on particles that moves with the fluid and store the dependent variables. The smoothed differential operators are, then, discretized through a set of particles that transport the main physical variables (e.g. pressure, velocity etc.). The way in which the continuous operators are represented at the discrete level leads to different schemes with different numerical properties.

At present, various works deal with the LES modelling in particle methods such as SPH[15–18]. Unfortunately, no rigorous derivation of such a procedure is provided, the LES closures being often included by directly rewriting the Eulerian differential operators in the SPH formalism. Further, most of the works that adopt LES approaches in SPH are applied to the modelling of wave breaking or complex free-surface flows for which the role played by LES terms is difficult to quantify. Recently, an attempt to validate an SPH model with LES closures has been made by Mayrhofer et al.[19] for a 3D channel flow. In the present paper, we want to reformulate, in a rigorous and general way, LES modelling in the SPH framework, in order to pave the way to a whole family of LES-SPH schemes. To this end, it is necessary to reformulate LES filtering in a Lagrangian context. This is done by using both a space and time filtering, this being the most general approach. This allows retaining the simple structure of the Lagrangian Navier–Stokes equations (where the material derivative of the velocity is proportional, via the mass, to the forces acting on the particle) and leads to additional terms in the filtered equations when adopting the SPH formalism, that must

be properly modelled to re–interpret SPH filtering as a sort of LES.

After proper closure formulas are provided (some prototypes are derived in the present work), the proposed LES-SPH model may be in principle capable of representing very challenging problems. Thanks to its Lagrangian structure, it may be suitable for the modelling of complex flows characterized by large deformations/fragmentations of the fluid domain (e.g. free-surface flows) and, at the same time, give a sound and reliable description of the turbulent effects.

The paper is organized as follows: the Navier–Stokes equation in Lagrangian formalism are recalled at first; Lagrangian Large Eddy Simulation with space–time filtering is then developed in section I; the SPH approximation of space operators is discussed in a LES perspective in section II while a classical test case for the free decay of two-dimensional turbulence is provided in section VI. Conclusions wrap up the paper. Details of Lagrangian filtering for LES are given in appendix.

I. LAGRANGIAN LARGE EDDY SIMULATION

In the present section, we cast the Large Eddy Simulation in a Lagrangian fashion. The resulting scheme is used in the sequel to define a general LES-SPH modelling.

In Lagrangian formalism, the Navier-Stokes equations for a barotropic weakly-compressible Newtonian fluid read:

$$
\begin{cases}
\dfrac{d\rho}{dt} = -\rho\,\nabla\cdot\boldsymbol{u}\,, \\[2em]
\dfrac{d\boldsymbol{u}}{dt} = -\dfrac{\nabla p}{\rho} + \nu\Delta\boldsymbol{u} + (\lambda' + \nu)\,\nabla\left(\nabla\cdot\boldsymbol{u}\right)\,, \\[2em]
\dfrac{d\boldsymbol{x}}{dt} = \boldsymbol{u}\,, \qquad p = F(\rho)\,,
\end{cases}
\tag{1}
$$

where $\boldsymbol{u}$ is the flow velocity, p and ρ denote the pressure and density fields respectively and F represents the state equation. The hypothesis that the fluid is weakly-compressible corresponds to assume:

$$
\frac{dp}{d\rho} = c^2 \gg \max\left(\,\|\boldsymbol{u}\|^2, \frac{p}{\rho}\right)\,,
\tag{2}
$$

where $c = c(\rho)$ is the sound speed (see e.g. Monaghan[20], Marrone et al.[21]). The viscosity coefficients ν, λ' indicate the ratios between the Lamé constants μ, λ and the density ρ. The

4

fluid being weakly-compressible, ν and λ' are assumed constant. For incompressible flows, equations (1) reduce to

$$
\begin{cases}
\nabla \cdot \boldsymbol{u} = 0, \qquad \rho = \text{constant}, \\[2em]
\dfrac{d\boldsymbol{u}}{dt} = -\dfrac{\nabla p}{\rho} + \nu \Delta \boldsymbol{u}, \\[2em]
\dfrac{d\boldsymbol{x}}{dt} = \boldsymbol{u},
\end{cases}
\tag{3}
$$

Now, let us define a Lagrangian filter with compact support in $\mathbb{R}^3 \times \mathbb{R}$ as follows:

$$
\phi = \phi \left(\tilde{\boldsymbol{x}}_p(t) - \boldsymbol{y}, t - \tau \right) .
\tag{4}
$$

The filter is supposed to depend only on $\|\tilde{\boldsymbol{x}}_p(t) - \boldsymbol{y}\|$ and $|t - \tau|$, and to be an even function with respect to both arguments. Here $\tilde{\boldsymbol{x}}_p(t)$ indicates the position of a material point that moves with the velocity

$$
\boxed{\tilde{\boldsymbol{u}} \left(\tilde{\boldsymbol{x}}_p(t), t \right) = \int_{\mathbb{R}^3} \int_{-\infty}^{+\infty} \phi \left(\tilde{\boldsymbol{x}}_p(t) - \boldsymbol{y}, t - \tau \right) \boldsymbol{u}(\boldsymbol{y}, \tau)\, d\tau\, dV_y ,}
\tag{5}
$$

that is:

$$
\tilde{\boldsymbol{x}}_p(t) = \int_{t_0}^{t} \tilde{\boldsymbol{u}} \left(\tilde{\boldsymbol{x}}_p(\tau), \tau \right)\, d\tau .
\tag{6}
$$

Hereinafter, we refer to $\tilde{\boldsymbol{x}}_p$ and $\tilde{\boldsymbol{u}}$ as the filtered position and velocity, respectively. We underline that, unless the turbulent process may be regarded as an ergodic one, the time and space filtering procedures are not equivalent and do not correspond to an ensemble averaging. The use of a space-time filter is the most general formulation for Lagrangian problems and is specifically suited for particle methods.

Since the state equation is generally nonlinear, $\widetilde{F(\rho)}$ is different from $F(\tilde{\rho})$ and, consequently, the filtering procedure cannot be applied to both pressure and density. To avoid inconsistency, when we refer to *filtered* pressure we mean

$$
\boxed{\tilde{p} = F(\tilde{\rho}) .}
\tag{7}
$$

Under this hypothesis, we apply the filter in (4) to the Navier-Stokes equations for weakly-compressible flows and, integrating over $\mathbb{R}^3 \times \mathbb{R}$, we obtain (see the appendix A for details):

$$
\begin{cases}
\dfrac{d\tilde{\rho}}{dt} = -\tilde{\rho}\,\nabla \cdot \tilde{\boldsymbol{u}} + \nabla \cdot \left[\tilde{\rho}\tilde{\boldsymbol{u}} - \widetilde{\rho\boldsymbol{u}}\right], \\[2mm]
\dfrac{d\tilde{\boldsymbol{u}}}{dt} = -\dfrac{\nabla \tilde{p}}{\tilde{\rho}} + \nu\Delta\tilde{\boldsymbol{u}} + (\lambda' + \nu)\,\nabla\left(\nabla \cdot \tilde{\boldsymbol{u}}\right) - \nabla\left[\widetilde{G(\rho)} - G(\tilde{\rho})\right] + \nabla \cdot \mathbb{T}_\ell + \widetilde{\boldsymbol{u}\,\nabla \cdot \boldsymbol{u}}, \\[2mm]
\dfrac{d\tilde{\boldsymbol{x}}_p}{dt} = \tilde{\boldsymbol{u}}, \qquad \tilde{p} = F\left(\tilde{\rho}\right), \qquad G(\rho) = \displaystyle\int^{\rho} \dfrac{1}{s}\dfrac{dF}{ds}\,ds,
\end{cases}
\tag{8}
$$

where

$$
\boxed{\mathbb{T}_\ell = \int_{\mathbb{R}^3}\int_{-\infty}^{+\infty}\phi\left(\tilde{\boldsymbol{x}}_p - \boldsymbol{y}, t - \tau\right)\left[\tilde{\boldsymbol{u}}(\tilde{\boldsymbol{x}}_p, t) - \boldsymbol{u}(\boldsymbol{y}, \tau)\right]\otimes\boldsymbol{u}(\boldsymbol{y}, \tau)\,dV_y d\tau = \tilde{\boldsymbol{u}}\otimes\tilde{\boldsymbol{u}} - \widetilde{\boldsymbol{u}\otimes\boldsymbol{u}}}.
$$

the tensor $\mathbb{T}_\ell$ being the Lagrangian equivalent of the sub-grid stress tensor. Note that the symbol d/dt now stands for the Lagrangian derivative following the filtered velocity field $\tilde{\boldsymbol{u}}$.

For incompressible flows (i.e. $\tilde{\rho} = \rho = const$ and $\tilde{p}$ indicates the filtered pressure field as in equation (5)), the system (8) simplifies to

$$
\begin{cases}
\nabla \cdot \tilde{\boldsymbol{u}} = 0, \\[2mm]
\dfrac{d\tilde{\boldsymbol{u}}}{dt} = -\dfrac{\nabla \tilde{p}}{\rho} + \nu\Delta\tilde{\boldsymbol{u}} + \nabla \cdot \mathbb{T}_\ell, \\[2mm]
\dfrac{d\tilde{\boldsymbol{x}}_p}{dt} = \tilde{\boldsymbol{u}},
\end{cases}
\tag{9}
$$

It is to be noticed that the choice of the space–time filter (4) yields a system of equations that retains the simple Lagrangian structure of the unfiltered Navier–Stokes equations (i.e. a system of equations where the time derivative is computed on fluid particles that move with the filtered velocity). The same structure can be obtained by using a simple space filter, even though a different closure is required for the additional terms as a consequence of the absence of the time filter.

Finally, we observe that the space-time filter in the Lagrangian context is formally identical to the analogous operation in the Eulerian context. Consequently, it can be verified that the formal relations between filtered quantities with different kernel supports (e.g. Germano's identity[22]) still hold true and can possibly be applied for the development of dynamic models.

II. SPH APPROXIMATION WITH A LES PERSPECTIVE

Using the results of the previous section, we are now in a position to define the main ingredients of a generic weakly-compressible LES-SPH model. First, we briefly recall the structure of SPH and, then, we proceed to the construction of the filtered LES-SPH equations.

The smoothing procedure used in all SPH approaches somehow recalls the one used to obtain the Lagrangian LES. The main differences between these filtering procedures is that SPH approaches adopt a filter ("kernel" in the SPH terminology) that depends only on the spatial variables $(\tilde{\boldsymbol{x}}_p - \boldsymbol{y})$; furthermore, the smoothing procedure is not applied to the Navier-Stokes equations, but rather to the differential operators, that are replaced by their smoothed counterpart (see Colagrossi et al.[13,14]).

It is possible, nevertheless, to reinterpret the Lagrangian LES through the SPH approach. To this purpose, we split the filter ϕ into

$$\phi\left(\tilde{\boldsymbol{x}}_p(t) - \boldsymbol{y}, t - \tau\right) = W(\tilde{\boldsymbol{x}}_p(t) - \boldsymbol{y})\,\theta(t - \tau)\,, \tag{10}$$

where W indicates the SPH kernel. In SPH notation, the smoothing procedure of a generic scalar field f is indicated as

$$\langle f\rangle\left(\tilde{\boldsymbol{x}}_p(t), t\right) = \int_{\mathbb{R}^3} W\left(\tilde{\boldsymbol{x}}_p(t) - \boldsymbol{y}\right) f(\boldsymbol{y}, t)\, dV_y\,. \tag{11}$$

Here, a time filtering alone is introduced by the symbol

$$\overline{f}\left(\boldsymbol{y}, t\right) = \int_{\mathbb{R}} \theta\left(t - \tau\right) f(\boldsymbol{y}, \tau)\, d\tau\,. \tag{12}$$

From the above definitions

$$
\begin{aligned}
\tilde{f} &= \int_{\mathbb{R}^3} \int_{-\infty}^{+\infty} \phi\left(\tilde{\boldsymbol{x}}_p(t) - \boldsymbol{y}, t - \tau\right) f\left(\boldsymbol{y}, \tau\right) d\tau\, dV_y \\
&= \int_{\mathbb{R}^3} W\left(\tilde{\boldsymbol{x}}_p(t) - \boldsymbol{y}\right)\left[\int_{-\infty}^{+\infty} \theta\left(t - \tau\right) f\left(\boldsymbol{y}, \tau\right) d\tau\right] dV_y \\
&= \int_{\mathbb{R}^3} W\left(\tilde{\boldsymbol{x}}_p(t) - \boldsymbol{y}\right) \overline{f}(\boldsymbol{y}, t)\, dV_y = \langle\,\overline{f}\,\rangle\,.
\end{aligned}
\tag{13}
$$

Note that, since $\tilde{\boldsymbol{x}}_p$ depends on time, time filtering and SPH smoothing (space filter) do not commute, i.e. $\langle\,\overline{f}\,\rangle \neq \overline{\langle f\rangle}$ (see, for example, the Appendix A 1). Since the time filter is the inner one, the overall LES-SPH scheme may be regarded as a spatial Lagrangian filter

applied to a set of time-averaged variables. In this sense, the time filter may be thought as an implicit filter whose presence is accounted for through the modeling of the additional terms.

Now, suppose that we want to compute a high Reynolds number flow, for which LES filtering is required. Then, we need the filtered variables $\tilde{\boldsymbol{u}}, \tilde{p}, \tilde{\rho}$ for each fluid particle at positions $\tilde{\boldsymbol{x}}_p$; at the same time, we want to approximate the operators in equation (8) in the SPH fashion. Considering the SPH approach (see the appendix A for details), we can write:

$$\nabla \cdot \tilde{\boldsymbol{u}} = \nabla \cdot \langle \overline{\boldsymbol{u}} \rangle = \langle \nabla \cdot \overline{\boldsymbol{u}} \rangle . \tag{14}$$

Of course, we cannot use time–filtered quantities like $\overline{\boldsymbol{u}}$ to approximate the operator, because we can compute only space-time filtered variables $\tilde{\boldsymbol{u}}, \tilde{\rho}, \tilde{p}$ associated to the particles at position $\tilde{\boldsymbol{x}}_p$ that move with speed $\tilde{\boldsymbol{u}}$. However, note that, far from the boundaries, differentiation and space filtering commute and the operator is linear; therefore, the divergence of the filtered velocity can be recast as

$$\nabla \cdot \tilde{\boldsymbol{u}} = \langle \nabla \cdot \overline{\boldsymbol{u}} \rangle = \langle \nabla \cdot (\overline{\boldsymbol{u}} + \tilde{\boldsymbol{u}} - \tilde{\boldsymbol{u}}) \rangle = \langle \nabla \cdot \tilde{\boldsymbol{u}} \rangle + \langle \nabla \cdot (\overline{\boldsymbol{u}} - \tilde{\boldsymbol{u}}) \rangle . \tag{15}$$

For confined flows, the non-commutability of filtering and differentiation must be taken into account for a rigorous extension of the filtering close to the boundaries (i.e. in those points whose distance from the boundaries is smaller than the kernel radius). The above procedure can be applied to all the remaining operators. By doing so, in SPH formalism the system (8) reads:

$$\begin{cases} \dfrac{d\tilde{\rho}}{dt} = -\tilde{\rho} \langle \nabla \cdot \tilde{\boldsymbol{u}} \rangle + \mathcal{C}_1 + \mathcal{C}_2 \,, \\[2em] \dfrac{d\tilde{\boldsymbol{u}}}{dt} = -\dfrac{\langle \nabla \tilde{p} \rangle}{\tilde{\rho}} + \nu \langle \Delta \tilde{\boldsymbol{u}} \rangle + (\lambda' + \nu) \langle \nabla (\nabla \cdot \tilde{\boldsymbol{u}}) \rangle + \mathcal{M}_1 + \mathcal{M}_2 \,, \\[2em] \dfrac{d\tilde{\boldsymbol{x}}_p}{dt} = \tilde{\boldsymbol{u}} \,, \qquad \tilde{p} = F(\tilde{\rho}) \,, \end{cases} \tag{16}$$

8

where:

$$\mathcal{C}_1 \,=\, -\tilde{\rho}\,\langle\,\nabla\cdot(\,\overline{\boldsymbol{u}}-\tilde{\boldsymbol{u}}\,)\,\rangle\,, \qquad \mathcal{C}_2 \,=\, \nabla\cdot[\,\tilde{\rho}\tilde{\boldsymbol{u}}-\widetilde{\rho\boldsymbol{u}}\,]\,, \tag{17}$$

$$\mathcal{M}_1 \,=\, -\frac{\langle\,\nabla\,(\,\overline{p}-\tilde{p}\,)\,\rangle}{\tilde{\rho}} \,+\, \nu\,\langle\,\Delta\,(\,\overline{\boldsymbol{u}}-\tilde{\boldsymbol{u}}\,)\,\rangle \,+\, (\lambda'+\nu)\,\langle\,\nabla\,(\,\nabla\cdot(\,\overline{\boldsymbol{u}}-\tilde{\boldsymbol{u}}\,)\,)\,\rangle\,, \tag{18}$$

$$\mathcal{M}_2 \,=\, -\nabla\left[\,\widetilde{G(\rho)}\,-\,G(\tilde{\rho})\,\right] \,+\, \widetilde{\boldsymbol{u}\,\nabla\cdot\boldsymbol{u}} \,+\, \nabla\cdot\mathbb{T}_\ell\,. \tag{19}$$

Here $\mathcal{C}_1$ and $\mathcal{M}_1$ come from the SPH approximation procedure and require a SPH closure, whereas $\mathcal{C}_2$ and $\mathcal{M}_2$ include all terms from the Lagrangian LES and require a LES closure. Incidentally, we note that the term $\mathcal{C}_2$ is not present in LES models for compressible flows where Favre-filtered variables are adopted (see, for example, Moin et al.[23]).

The filtered functions can be split as

$$\tilde{\boldsymbol{u}} = \overline{\boldsymbol{u}} + \boldsymbol{u}'\,, \qquad\qquad \tilde{p} = \overline{p} + p'\,. \tag{20}$$

where $\boldsymbol{u}', p'$ represent small scale "fluctuations" in space. By doing so, $\mathcal{C}_1$ and $\mathcal{M}_1$ can be rewritten as

$$\mathcal{C}_1 \,=\, \tilde{\rho}\,\langle\,\nabla\cdot\boldsymbol{u}'\,\rangle\,, \qquad\qquad \mathcal{M}_1 \,=\, \frac{\langle\,\nabla p'\,\rangle}{\tilde{\rho}} \,-\, \nu\,\langle\,\Delta\boldsymbol{u}'\,\rangle \,-\, (\lambda'+\nu)\,\langle\,\nabla\,(\,\nabla\cdot\boldsymbol{u}'\,)\,\rangle\,. \tag{21}$$

The system (16) can be regarded as a general LES-SPH model. The specific closures adopted for terms $\mathcal{C}_1, \mathcal{C}_2, \mathcal{M}_1$ and $\mathcal{M}_2$ will define a whole family of methods based on a consistent inclusion of the LES approach in the SPH framework.

III.   CLOSURES FOR $\mathcal{C}_1$ AND $\mathcal{M}_1$

In this section we provide some estimates for the terms $\mathcal{C}_1$ and $\mathcal{M}_1$ of the LES-SPH model in (16). Let us consider a scalar field f and its Taylor expansion:

$$f(\boldsymbol{y}) \,=\, f(\boldsymbol{x}) \,+\, \nabla f\big|_{\boldsymbol{x}}\cdot(\boldsymbol{y}-\boldsymbol{x}) \,+\, \frac{1}{2}(\boldsymbol{y}-\boldsymbol{x})\cdot\mathbb{H}[f]\big|_{\boldsymbol{x}}\cdot(\boldsymbol{y}-\boldsymbol{x}) \,+\, \mathcal{O}\left(\|\boldsymbol{y}-\boldsymbol{x}\|^3\right)\,, \tag{22}$$

where the tensor $\mathbb{H}[f]$ indicates the Hessian of the function f, namely $\mathbb{H}_{ij} = \partial^2 f/\partial x_i\partial x_j$. Applying the spatial filter and using its standard properties, we immediately obtain:

$$\langle f\rangle \,=\, f \,+\, \alpha\,h^2\,\Delta f \,+\, \mathcal{O}(h^4)\,, \tag{23}$$

9

and, substituting the leading order in the Laplacian, we also find:

$$\langle f \rangle = f + \alpha\, h^2\, \Delta\langle f \rangle + \mathcal{O}(h^4)\,. \tag{24}$$

Here, h is a reference length of the spatial filter support (generally denoted smoothing length in the SPH literature) and α is a positive dimensionless parameter defined as follows:

$$\int_{\mathbb{R}^3} (\boldsymbol{y} - \boldsymbol{x}) \otimes (\boldsymbol{y} - \boldsymbol{x})\, W(\boldsymbol{x} - \boldsymbol{y})\, dV_y = 2\,\alpha\, h^2\, \mathbb{1}\,. \tag{25}$$

Following the works of Violeau and Leroy[24] and Dehnen and Aly[25], we use the standard deviation $\sigma = \sqrt{\alpha}\, h$ as a reference length for the SPH filtering procedure instead of h. Using equation (24), we obtain:

$$\boldsymbol{u}' = \tilde{\boldsymbol{u}} - \overline{\boldsymbol{u}} = \langle \overline{\boldsymbol{u}} \rangle - \overline{\boldsymbol{u}} = \sigma^2\, \Delta\langle \overline{\boldsymbol{u}} \rangle + \mathcal{O}(\sigma^4)\,, \qquad p' = \tilde{p} - \overline{p} = \langle \overline{p} \rangle - \overline{p} = \sigma^2\, \Delta\langle \overline{p} \rangle + \mathcal{O}(\sigma^4)\,,$$

that is:

$$\boldsymbol{u}' = \tilde{\boldsymbol{u}} - \overline{\boldsymbol{u}} = \sigma^2\, \Delta\tilde{\boldsymbol{u}} + \mathcal{O}(\sigma^4)\,, \qquad p' = \tilde{p} - \overline{p} = \sigma^2\, \Delta\tilde{p} + \mathcal{O}(\sigma^4)\,.$$

The above relations allows us to estimate the terms $\mathcal{C}_1$ and $\mathcal{M}_1$ defined in equation (21). Specifically, substituting them in the definition of $\mathcal{C}_1$ and retaining the leading-order term, we find:

$$\mathcal{C}_1 \simeq \tilde{\rho}\, \langle \nabla \cdot \left(\sigma^2 \Delta\tilde{\boldsymbol{u}}\right) \rangle\,, \tag{26}$$

where the right-hand side represents the closure for $\mathcal{C}_1$. Substituting the above expression in the continuity equation of the system (16) and using equation (24), we obtain:

$$\frac{d\tilde{\rho}}{dt} = -\tilde{\rho}\, \langle \nabla \cdot \left(\tilde{\boldsymbol{u}} - \sigma^2 \Delta\tilde{\boldsymbol{u}}\right) \rangle + \mathcal{C}_2 = -\tilde{\rho}\, \langle \nabla \cdot \overline{\boldsymbol{u}} \rangle + \mathcal{O}(\sigma^4) + \mathcal{C}_2 = -\tilde{\rho}\, \nabla \cdot \tilde{\boldsymbol{u}} + \mathcal{O}(\sigma^4) + \mathcal{C}_2\,.$$

Similarly, applying the same procedure to estimate $\mathcal{M}_1$, we can rearrange the momentum equation of the system (16) as follows:

$$\frac{d\tilde{\boldsymbol{u}}}{dt} = -\frac{\langle \nabla\overline{p} \rangle}{\tilde{\rho}} + \nu\langle \Delta\overline{\boldsymbol{u}} \rangle + (\lambda' + \nu)\, \langle \nabla(\nabla \cdot \overline{\boldsymbol{u}}) \rangle + \mathcal{O}(\sigma^4) + \mathcal{M}_2 =$$

$$= -\frac{\nabla\tilde{p}}{\tilde{\rho}} + \nu\Delta\tilde{\boldsymbol{u}} + (\lambda' + \nu)\, \nabla(\nabla \cdot \tilde{\boldsymbol{u}}) + \mathcal{O}(\sigma^4) + \mathcal{M}_2\,,$$

confirming that the overall accuracy of the SPH approximation is $\mathcal{O}(\sigma^4)$.

IV.   CLOSURES FOR $\mathcal{C}_2$ AND $\mathcal{M}_2$

For what concerns $\mathcal{C}_2$ and $\mathcal{M}_2$, we adopt a typical LES modelling. Note that this corresponds to neglecting the action of the time filter, that, in any case, can be taken into account with more general and complex closures for $\mathcal{C}_2$ and $\mathcal{M}_2$. For the time being, following Yoshizawa[26] we write:

$$\mathcal{M}_2 = \nabla \cdot \mathbb{T}_\ell = \nabla \cdot \left[-\frac{q^2}{3}\,\mathbb{1} \, - \, \frac{2}{3}\,\nu_T\, \mathrm{Tr}(\widetilde{\mathbb{D}})\,\mathbb{1} \, + \, 2\,\nu_T\,\widetilde{\mathbb{D}} \right] , \qquad (27)$$

where q^2 represents the turbulent kinetic energy, ν_T is the turbulent kinetic viscosity and $\widetilde{\mathbb{D}}$ is the strain-rate tensor, that is $\widetilde{\mathbb{D}} = (\nabla \tilde{\boldsymbol{u}} + \nabla \tilde{\boldsymbol{u}}^T)/2$. Similarly to Yoshizawa[26], we assume:

$$q^2 \, = \, 2\, C_Y\, \sigma^2 \, \| \, \widetilde{\mathbb{D}} \, \|^2 , \qquad \nu_T \, = \, (C_S\, \sigma)^2\, \| \, \widetilde{\mathbb{D}} \, \| , \qquad (28)$$

where $\|\widetilde{\mathbb{D}}\|$ is a rescaled Frobenius norm, namely:

$$\| \, \widetilde{\mathbb{D}} \, \| \, = \, \sqrt{2\,\widetilde{\mathbb{D}} \!:\! \widetilde{\mathbb{D}}} \ . \qquad (29)$$

The dimensionless parameters C_Y and C_S are respectively called the Yoshizawa and Smagorinsky constants. In Yoshizawa[26] $C_Y = 0.044$ is used while, regarding the Smagorinsky constant, $C_S = 0.12$ has been adopted like in Lo and Shao[17] and in Dalrymple and Rogers[18]. Note that the first two terms in expression (19) for $\mathcal{M}_2$ are neglected based on the low Mach number flow assumption (i.e. Ma< 0.1). For a general discussion on the influence of compressibility in turbulent flows see e.g. Blaisdell et al.[41], Passot et al.[42]. Further, as commented in Suh et al.[43], also the first two terms in equation (27) are not relevant for the same reasons.

For what concerns the term $\mathcal{C}_2$, we follow a similar approach and assume a Fick-like diffusion law. Specifically, we put:

$$\mathcal{C}_2 \, = \, \nabla \cdot \left[\, \tilde{\rho}\tilde{\boldsymbol{u}} - \widetilde{\rho \boldsymbol{u}} \, \right] \, = \, \nabla \cdot \left(\, \nu_\delta\, \nabla \tilde{\rho} \right) , \qquad (30)$$

where ν_δ has the dimension of a kinetic viscosity and represents a turbulent diffusion coefficient. Similarly to the expression of ν_T, we assume the following structure:

$$\nu_\delta \, = \, (C_\delta\, \sigma)^2 \, \| \, \widetilde{\mathbb{D}} \, \| , \qquad (31)$$

where C_δ is a dimensionless coefficient. This has been set equal to 1.5 after some preliminary numerical experiments. A complete calibration is postponed to future works.

If the spatial derivatives of ν_δ are negligible, the above expression simplifies as follows:

$$\mathcal{C}_2 = \nu_\delta \, \Delta \tilde{\rho} \,. \tag{32}$$

This structure of $\mathcal{C}_2$ is practically identical to the diffusive term proposed by Molteni and Colagrossi[27]. Both formulas in (27) and (30) have been modelled by using the standard SPH differential operators. The details of the numerical implementation are described in the following section.

V. NUMERICAL IMPLEMENTATION

Here we provide the details about the numerical implementation of the LES-SPH model. The differential operators have been discretized through the expressions usually adopted for the weakly-compressible SPH schemes (see, for example, Colagrossi et al.[13,14], Le Touzé et al.[28]). Then, the discrete scheme reads:

$$\begin{cases} \dfrac{d\tilde{\rho}_i}{dt} = -\tilde{\rho}_i \sum_j \left(\overline{\boldsymbol{u}}_j - \overline{\boldsymbol{u}}_i \right) \cdot \nabla_i W_{ij} \, V_j + \mathcal{C}_2^{(i)} \,, \\[2ex] \dfrac{d\tilde{\boldsymbol{u}}_i}{dt} = -\dfrac{1}{\tilde{\rho}_i} \sum_j \left(\overline{p}_j + \overline{p}_i \right) \nabla_i W_{ij} \, V_j + \boldsymbol{f}_i + \dfrac{\mu}{\tilde{\rho}_i} \sum_j \overline{\pi}_{ij} \, \nabla_i W_{ij} \, V_j + \mathcal{M}_2^{(i)} \,, \\[2ex] \dfrac{d\tilde{\boldsymbol{x}}_i}{dt} = \tilde{\boldsymbol{u}}_i \,, \qquad \tilde{p}_i = c_0^2 \left(\tilde{\rho}_i - \tilde{\rho}_0 \right) \,, \qquad V_i = m_i / \tilde{\rho}_i \,. \end{cases} \tag{33}$$

where μ, c_0 and ρ_0 indicate respectively the dynamic viscosity, the selected speed of sound and the reference density. To satisfy the weakly-compressible assumption, c_0 is chosen to be at least one order of magnitude greater than the maximum flow velocity (see Marrone et al.[21] for details). The subscript 'i' indicates the quantities associated with the i-th particle at the position $\tilde{\boldsymbol{x}}_i$. Conversely, the letter 'j' is used for a generic quantity associated with a particle which is inside the compact support of the SPH kernel, i.e. $W_{ij} = W(\tilde{\boldsymbol{x}}_i - \tilde{\boldsymbol{x}}_j)$. Consistently, the gradient ∇_i indicates the differentiation with respect to $\tilde{\boldsymbol{x}}_i$, the symbols $\tilde{\rho}_i$ and V_i are respectively the density and the volume of the i-th particle while the vector $\boldsymbol{f}_i$ represents a generic body force acting on the i-th particle. The particle mass, namely m_i, is maintained constant during the flow evolution, thus ensuring the global mass conservation. The filtered pressure and velocity of the i-th particle are denoted through $\tilde{p}_i$ and $\tilde{\boldsymbol{u}}_i$, while,

in accordance with the results of Section III, $\bar{p}_i$ and $\overline{\boldsymbol{u}}_i$ are expressed as follows:

$$\bar{p}_i \;=\; \tilde{p}_i \,-\, \sigma^2 \,\Delta \tilde{p}_i \;=\; \tilde{p}_i \,-\, 2\,\sigma^2 \sum_j \left(\,\tilde{p}_j - \tilde{p}_i\,\right) \frac{\tilde{\boldsymbol{x}}_{ji} \cdot \nabla_i W_{ij}}{\|\tilde{\boldsymbol{x}}_{ji}\|^2}\, V_j\,, \tag{34}$$

$$\overline{\boldsymbol{u}}_i \;=\; \tilde{\boldsymbol{u}}_i \,-\, \sigma^2 \,\Delta \tilde{\boldsymbol{u}}_i \;=\; \tilde{\boldsymbol{u}}_i \,-\, 2\,\sigma^2 \sum_j \left(\,\tilde{\boldsymbol{u}}_j - \tilde{\boldsymbol{u}}_i\,\right) \frac{\tilde{\boldsymbol{x}}_{ji} \cdot \nabla_i W_{ij}}{\|\tilde{\boldsymbol{x}}_{ji}\|^2}\, V_j\,, \tag{35}$$

where $\tilde{\boldsymbol{x}}_{ji} = (\tilde{\boldsymbol{x}}_j - \tilde{\boldsymbol{x}}_i)$ and the Morris et al.[29] formula has been adopted for the Laplacian. As discussed in Section III, the above formulas leads to an overall approximation of order $\mathcal{O}(\sigma^4)$. The symbol $\overline{\pi}$ indicates the molecular viscosity term (see Monaghan[2]) expressed as function of $\overline{\boldsymbol{u}}$ according to the results of Section III. It reads:

$$\overline{\pi}_{ij} \;=\; K\, \frac{(\,\overline{\boldsymbol{u}}_j - \overline{\boldsymbol{u}}_i\,) \cdot \tilde{\boldsymbol{x}}_{ji}}{\|\,\tilde{\boldsymbol{x}}_{ji}\,\|^2}\,, \tag{36}$$

where $K = 2(n+2)$ and n is the number of spatial dimensions. For what concerns $\mathcal{C}_2^{(i)}$ and $\mathcal{M}_2^{(i)}$, we use the following expressions (see Section §IV):

$$\mathcal{C}_2^{(i)} \;=\; 4 \sum_j \left(\frac{\nu_\delta^{(i)}\, \nu_\delta^{(j)}}{\nu_\delta^{(i)} + \nu_\delta^{(j)}} \right) (\,\tilde{\rho}_j - \tilde{\rho}_i\,) \frac{\tilde{\boldsymbol{x}}_{ji} \cdot \nabla_i W_{ij}}{\|\tilde{\boldsymbol{x}}_{ji}\|^2}\, V_j\,, \tag{37}$$

$$\mathcal{M}_2^{(i)} \;=\; -\sum_j \left(q_j^2 + q_i^2 \right) \nabla_i W_{ij}\, V_j \,+\, 2 \sum_j \left(\frac{\nu_T^{(i)}\, \nu_T^{(j)}}{\nu_T^{(i)} + \nu_T^{(j)}} \right) \tilde{\pi}_{ij}\, \nabla_i W_{ij}\, V_j\,. \tag{38}$$

These derive from a straightforward generalization of the Laplacian of Morris et al.[29] and of the viscous term of Monaghan[2]. Note that $\tilde{\pi}_{ij}$ is evaluated by using $\tilde{\boldsymbol{u}}_i$ instead of $\overline{\boldsymbol{u}}_i$. The expressions for $q_i^2, \nu_T^{(i)}$ and $\nu_\delta^{(i)}$ are given in equations (28) and (31) while the strain-rate tensor is computed through the formula below (see Colagrossi et al.[14]):

$$\widetilde{\mathbb{D}}_i \;=\; \frac{1}{2} \sum_j \left[\, (\tilde{\boldsymbol{u}}_j - \tilde{\boldsymbol{u}}_i) \otimes (\mathbb{L}_i \cdot \nabla W_{ij}) + (\mathbb{L}_i \cdot \nabla W_{ij}) \otimes (\tilde{\boldsymbol{u}}_j - \tilde{\boldsymbol{u}}_i) \,\right] V_j\,, \tag{39}$$

where $\mathbb{L}_i$ indicates the gradient renormalization tensor:

$$\mathbb{L}_i \;=\; \left[\sum_j \tilde{\boldsymbol{x}}_{ji} \otimes \nabla W_{ji}\, V_j \right]^{-1}\,, \tag{40}$$

which guarantees the first order completeness for the equation (39) (for details see[30]). The C2 Wendland kernel has been chosen for the spatial filter W (see *e.g.* Colagrossi et al.[31]), this implying $\alpha = 5/18$ [see equation (25)], and a fourth-order Runge-Kutta scheme has been implemented to advance in time the model. Furthermore, the packing algorithm described in

Colagrossi et al.[32] has been used to obtain the so-called "glass-configurations" for the initial particle positions. The main characteristic of these configurations is that the particle inter-distance is close to the mean global value Δx. Consequently, it is possible to associate the same initial volume, namely Δx^2, to all particles even if their distribution is not perfectly regular. These configurations are preferable to the Cartesian lattice since they avoid the particle resettlement during the early stages of the evolution (see Antuono et al.[33]). A ratio $\sigma/\Delta x = 2\sqrt{\alpha}$ is used in all the simulations, this corresponding to about 50 particles (in 2D) in the kernel support. In order to evaluate the energy spectrum during the post-processing stage, the magnitude of the velocity fields have been interpolated on a uniform Cartesian mesh with spacing equal to Δx. For the interpolation of the SPH scattered data, a Moving Least Square technique has been used as described in Shi et al.[34].

VI.   NUMERICAL RESULTS: A PROOF OF CONCEPT

A.   Freely-decaying turbulence in 2D

As a proof of concept of the modelling outlined above, we report some simulations of free decay of two dimensional homogeneous turbulence, with different values of the viscosity and various discretizations. An exhaustive and in-depth analysis of this preliminary numerical scheme is out of the scope of the present work and is postponed to future studies.

The initial conditions were chosen similarly to those of the physical experiment described in Tabeling[35] for a regular configuration with 64 vortices. These were cast in an array of 8×8 Taylor–Green vortices in a bi-periodic domain with size $L \times L$ (the reference length L is set equal to 1). The maximum value of the velocity field in the initial configuration is $U = 1$ while a positive constant value, namely $P_0 = 2\,\rho_0\,U^2$, has been added to the pressure field to avoid the onset of the so-called "tensile-instability" (see Swegle et al.[36]). The initial vorticity and pressure are shown in figure 1.

In the first simulation, the Reynolds number was $Re_l = lU/\nu = 1250$, with $l = L/8$ the vortex size. The turbulent field is displayed in figure 2 in terms of vorticity distribution at the non dimensional time $tU/L = 3$, for both a DNS and a LES simulation. In this case, a direct simulation is still feasible with a discretization $l/\sigma = 144$, as shown in figure 3 (here σ^2 indicates the second momentum of the spatial filter W as defined in Section III).

14

In fact, the direct simulation is able to capture the main features of the energy spectrum predicted by the Kraichnan's theory (see Kraichnan[37]) and the direct and inverse energy cascades with slope -3 and $-5/3$ are visible in both simulations. For this value of the Reynolds number, the direct simulation shows a flattening of the spectrum for large wave numbers (i.e. above $kL > 200$). This behaviour is typical of the standard SPH scheme and
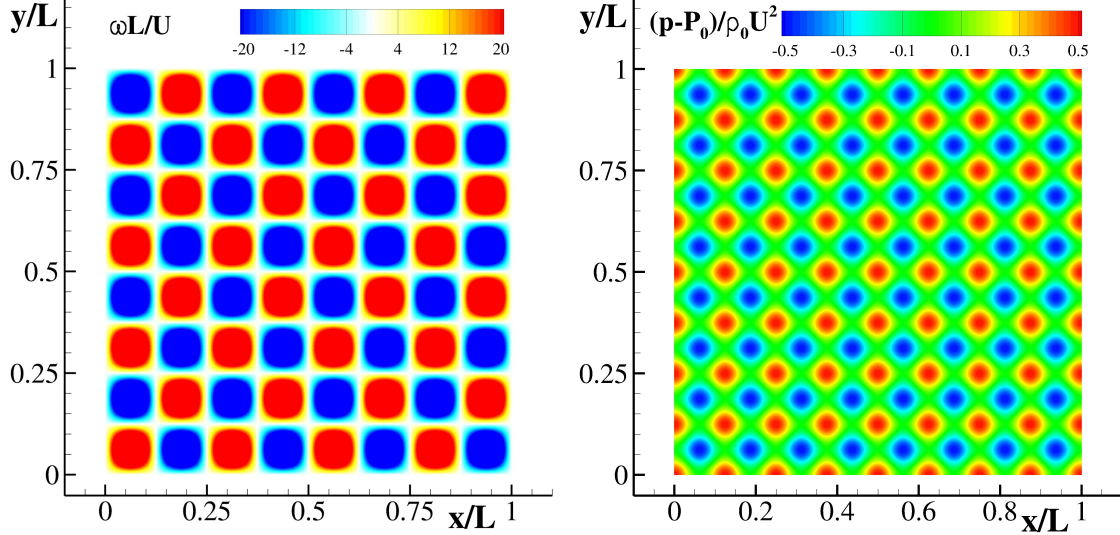

FIG. 1. Two-dimensional freely-decaying turbulence. Initial configuration: vorticity (left) and pressure (right) fields.
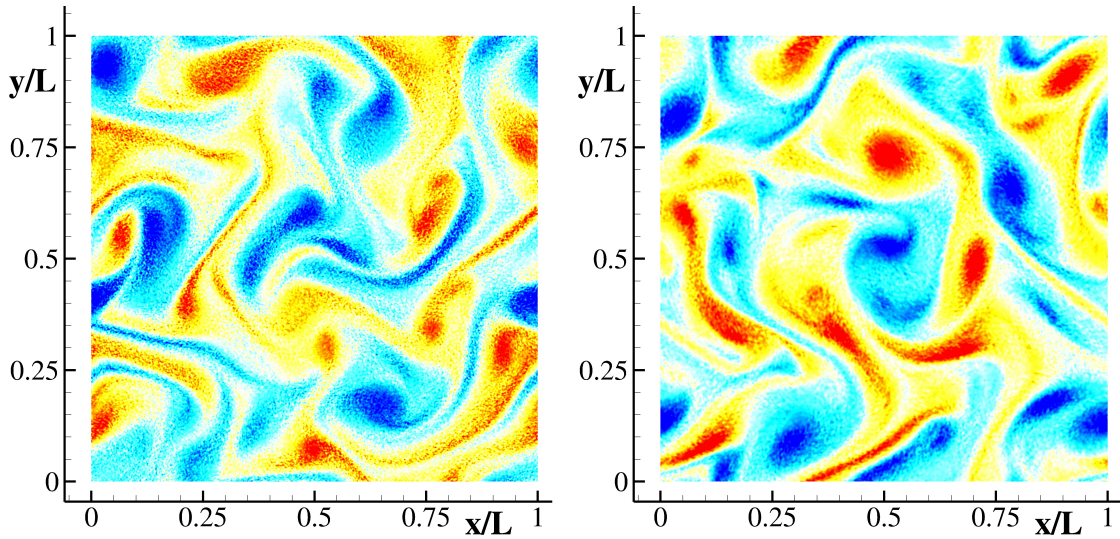
FIG. 2. Two-dimensional freely-decaying turbulence at $\mathrm{Re}_l = 1250$. Vorticity field at non-dimensional time $tU/L = 3$, DNS-SPH (left), LES-SPH (Right).

is not caused by an insufficient spatial discretization, but rather by a spurious energy flux towards high frequencies. This has been explained in Ellero et al.[38], as heuristically shown in Colagrossi et al.[31]. On the contrary, the LES modelling seems to prevent and attenuate this non-physical behaviour, and, at the same time, gives a correct representation of the theoretical energy spectra for lower wave numbers.

Far more interesting is the simulation with $Re_l = 125,000$. For this case, three different particle discretizations were adopted, namely $l/\sigma = 18, 36, 144$. These are all insufficient for a correct direct simulation through the standard SPH scheme but are fine enough for the proposed LES-SPH model. This is confirmed by the energy spectra of figure 4, where the three discretizations are reported. For the two coarser particle resolutions, the energy distribution in frequency of the standard SPH is completely unrealistic, the slope of the spectrum being even opposite to the expected one in most of the range. On the contrary, the finest discretization is able to reproduce the correct energy distribution up to $kL \sim 30$, while for higher frequencies the spectrum attains a non-physical plateau that unveils a dissipation connected with the numerical approximation rather than with physical phenomena. Conversely, when performing LES simulations, the portion of the spectrum connected with inverse cascade (i.e. slope $-5/3$) is correctly captured with all the particle
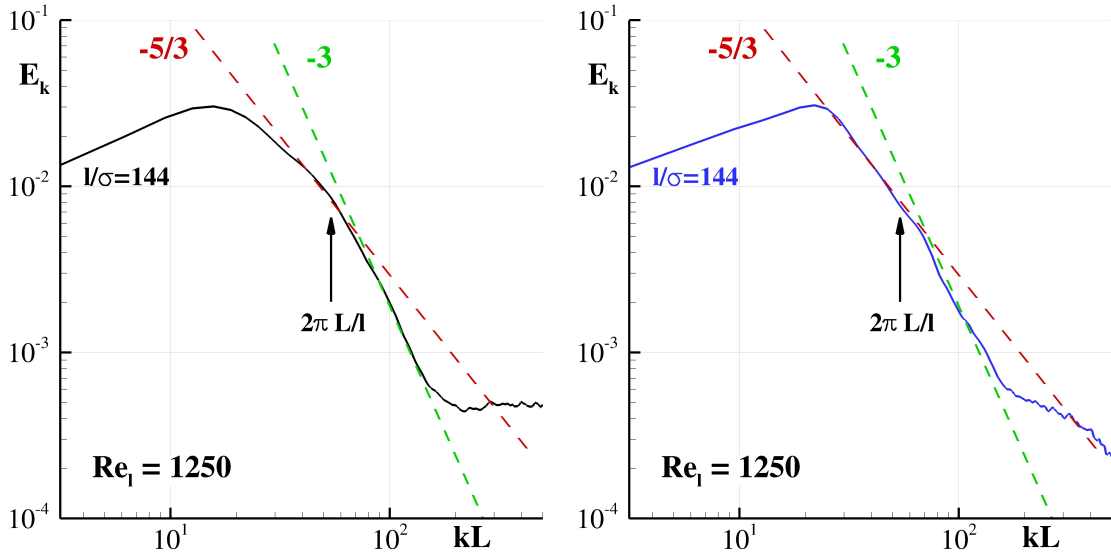

FIG. 3. Two-dimensional freely-decaying turbulence at non-dimensional time $tU/L = 3$ for $Re_l = 1250$. Left: energy spectrum from a DNS-SPH simulation. Right: energy spectrum from a LES-SPH simulation.

spacings adopted, while for higher frequencies the energy content quickly drops, because of modelling effects. As expected, the amount of resolved energy increases when refining the discretization, as shown by the upward shift of the curves. Figure 5 shows the computed vorticity field at the dimensionless time $tU/L = 2$ by both DNS and LES simulations; in the former case the amount of non-physical noise on the solution is clearly visible in the left plot. The increase of resolved energy with finer discretizations is further confirmed by the values of the eddy viscosity, displayed in figure 6. In fact, for $l/\sigma = 18$ the computed maximum eddy viscosity was 60 times larger than the physical viscosity; for the finest resolution, this ratio drops to about 2.

For a chosen spatial resolution, we observe an increase of about 30% of the computational costs of the LES-SPH models with respect to the simulations without the additional terms $\mathcal{C}_1$, $\mathcal{M}_1$, $\mathcal{C}_2$ and $\mathcal{M}_2$.

1. *Comparison with an existing SPH model*

Here we show a comparison with the SPH model described in Dalrymple and Rogers[18], this corresponding to the present LES-SPH scheme if $\mathcal{C}_1$, $\mathcal{M}_1$ and $\mathcal{C}_2$ are set to zero.
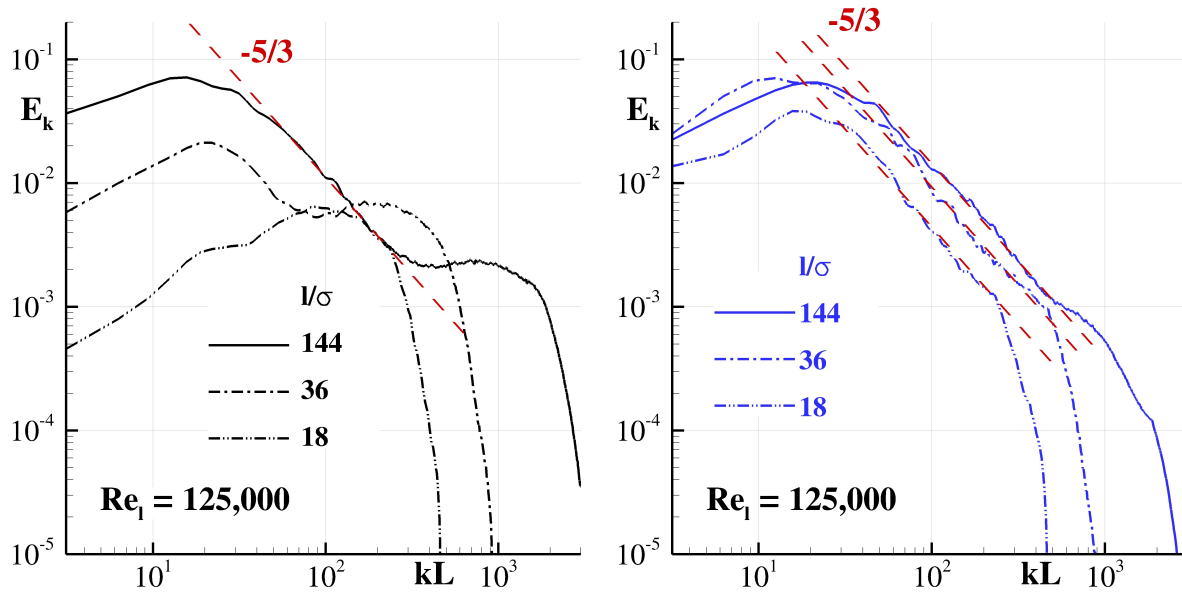

FIG. 4.   Two-dimensional freely-decaying turbulence at non-dimensional time $tU/L = 2$ for $\mathrm{Re}_l = 125,000$. Left: energy spectrum from a DNS-SPH simulation. Right: energy spectrum from a LES-SPH simulation.
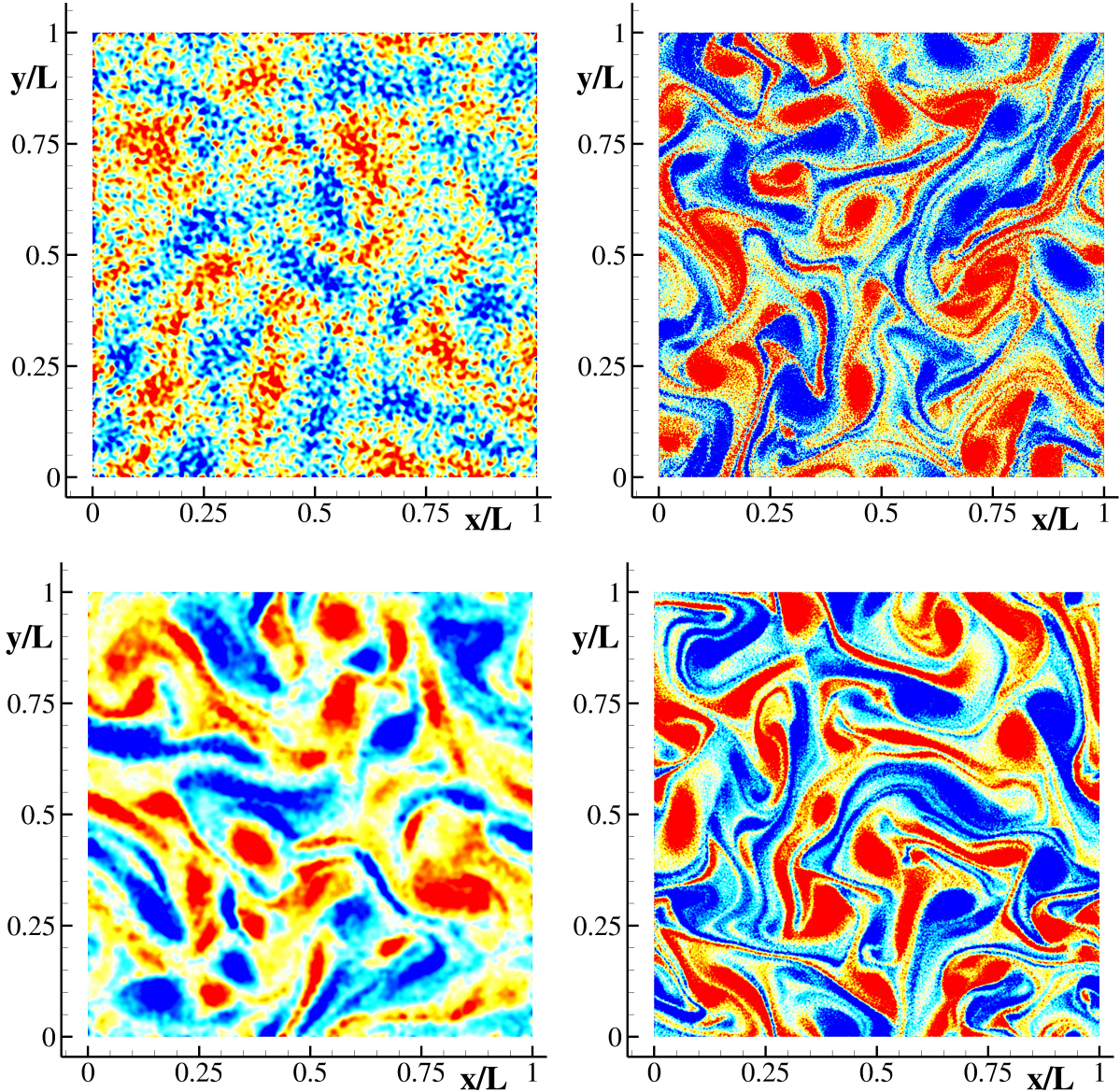
FIG. 5. Two-dimensional freely-decaying turbulence at $Re_l = 125,000$. Vorticity field at non-dimensional time $tU/L = 2$. Top: DNS-SPH using spatial resolution l/σ equal to 36 (left) and 144(right). Bottom: LES-SPH using spatial resolution l/σ equal to 36 (left) and 144(right).

Figure 7 displays the energy spectrum obtained by using the model of Dalrymple and Rogers[18] (black lines) and the proposed LES-SPH scheme (blue lines) for $Re_l = 1250$ (left panel) and $Re_l = 125,000$ (right panel). In the former case, the behaviour of the spectrum in the inertial range is correctly described by both the models, while for the largest Reynolds number the scheme of Dalrymple and Rogers[18] displays non-physical kinetic energy content for high wave numbers.
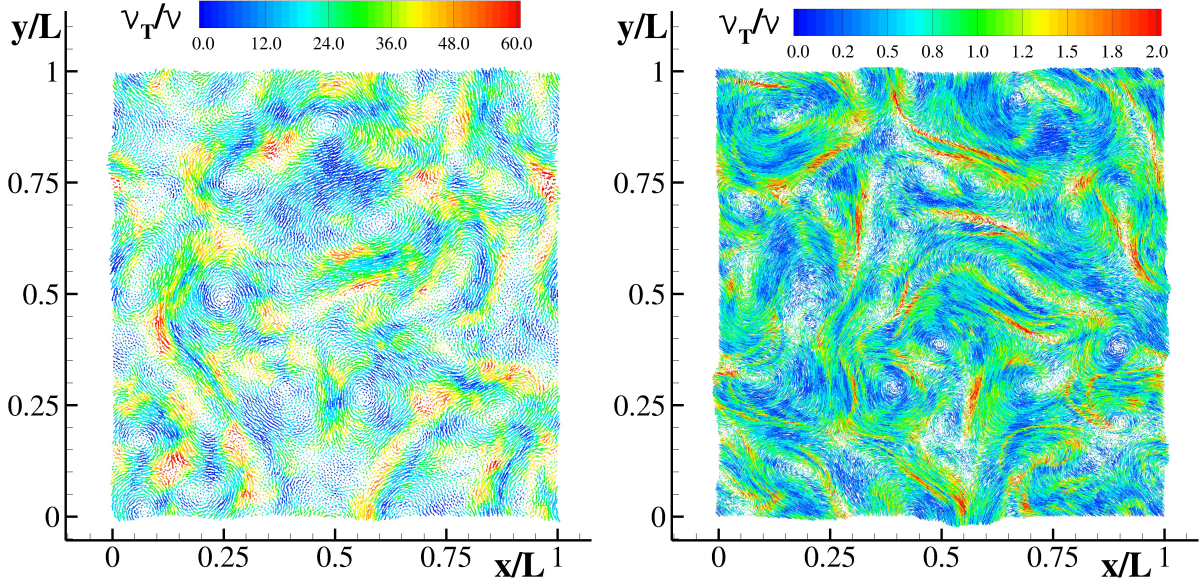
FIG. 6. Two-dimensional freely-decaying turbulence at $\text{Re}_l = 125,000$. Contour plot of the ratio ν_T/ν at non dimensional time $tU/L = 2$, using different spatial resolutions $l/\sigma = 18$ (left) and $l/\sigma = 144$ (right).
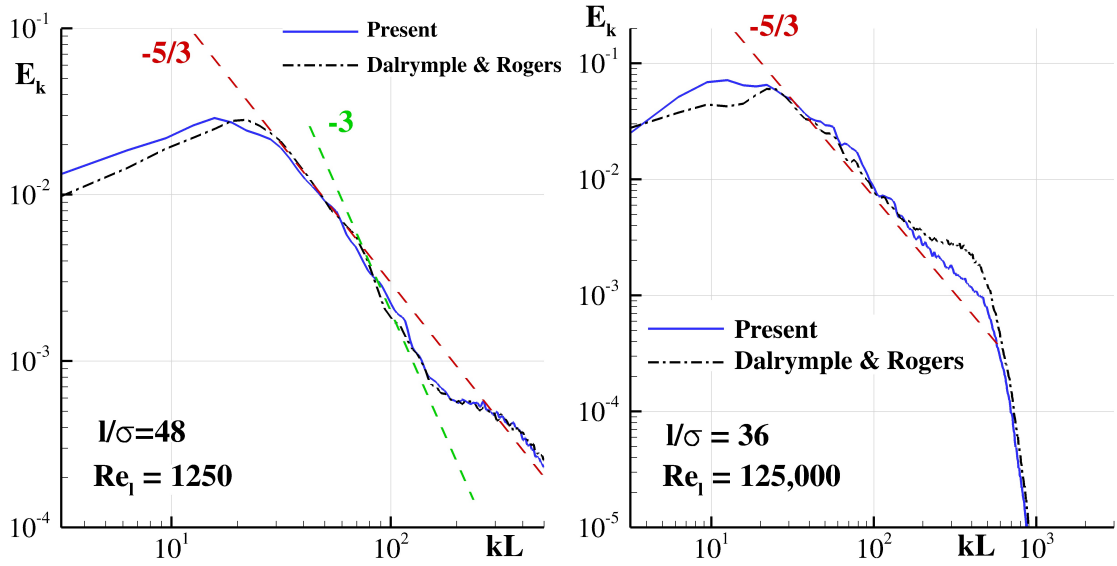

FIG. 7. Two-dimensional freely decay turbulence. The energy spectrum obtained by using the model of Dalrymple and Rogers[18] (black lines) and the proposed SPH-LES scheme (blue lines) for $Re_l = 1250$ (left panel) and $Re_l = 125,000$ (right panel).

This difference is mainly due to the action of the term $\mathcal{C}_2$ which, similarly to the diffusive term in the δ-SPH scheme of Antuono et al.[40], allows for a drastic reduction of spurious
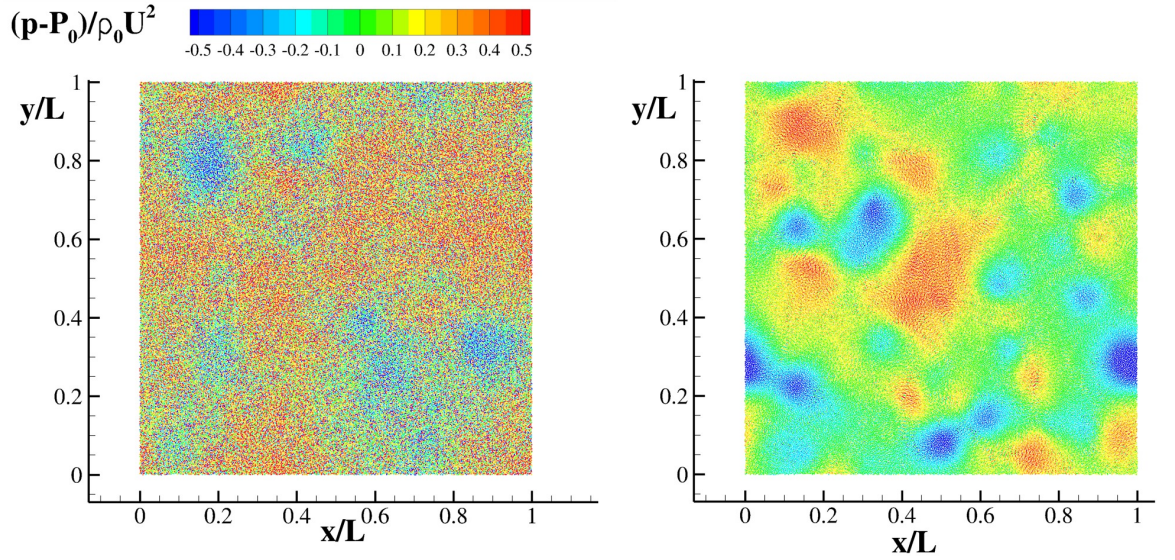
FIG. 8. Two-dimensional freely decay turbulence. The pressure field for $Re_l = 125,000$ as predicted by the model of Dalrymple and Rogers[18] (left) and by the proposed LES-SPH scheme (right).

high-frequency oscillations that generally affect the weakly-compressible SPH schemes. The effects of the action of $\mathcal{C}_2$ are displayed in figure 8 where the pressure field predicted by the two models is compared at $tU/L = 2$ for $Re_l = 125,000$. The left panel shows the results obtained by using the model of Dalrymple and Rogers[18] while the right panel displays the results of the present model.

The terms $\mathcal{C}_1$ and $\mathcal{M}_1$ generally play a secondary role. They principally act in opposition to $\mathcal{C}_2$ and $\mathcal{M}_2$ since they behave as anti-diffusive terms [see equation (26)]. Specifically, they limit the dissipation induced by $\mathcal{C}_2$ and $\mathcal{M}_2$ at high frequencies.

B.   Decay of homogeneous turbulence in 3D

As a proof of concept for the proposed filtering in three dimensions, in the present section we report the simulations of homogeneous turbulence for various values of the Reynolds number. The simulations are carried out in a tri-periodic box, namely $0 < x_i < 2\pi L$ with $i = 1, 2, 3$ and $L = 1$, and the initial conditions are generated in the Fourier space as in Mansour and Wray[39].

In particular, the Fourier components of the velocity are computed as

$$\hat{\boldsymbol{u}}_i(\boldsymbol{\kappa}) = \alpha \boldsymbol{e}_i^1 + \beta \boldsymbol{e}_i^2 \,, \tag{41}$$

where $\boldsymbol{e}_i^1$ and $\boldsymbol{e}_i^2$ are two mutually orthogonal unit vector in the plane orthogonal to the wave vector $\boldsymbol{\kappa}$. The complex coefficients α and β are given by:

$$\alpha = \frac{E(\kappa)}{4\pi\kappa^2} \exp\left(i\theta_1\right) \cos\left(\phi\right) , \qquad \beta = \frac{E(\kappa)}{4\pi\kappa^2} \exp\left(i\theta_2\right) \sin\left(\phi\right) , \tag{42}$$

where θ_1, θ_2 and ϕ are uniformly distributed random numbers on the interval $(0, 2\pi)$ and $\kappa = |\boldsymbol{\kappa}|$. The spectrum $E(\kappa)$ is assumed as

$$E(\kappa) = \frac{q^2}{2A} \frac{\kappa^\varsigma}{\kappa_p^{\varsigma+1}} \exp\left[-\frac{\varsigma}{2}\left(\frac{\kappa}{\kappa_p}\right)^2\right] , \tag{43}$$

where $\kappa_p = 9$ is the wave number at which the spectrum is maximum, $\varsigma = 4$, $q^2 = 3$ and A is computed so that the initial turbulence intensity is unitary. This value U is taken as reference velocity. Since the actual computation is in the real space, the velocity vector is computed as:

$$\tilde{\boldsymbol{u}}(\tilde{\boldsymbol{x}}_p, 0) = \Re\left(\mathcal{F}^{-1}[\hat{\boldsymbol{u}}]\right) \tag{44}$$

where $\mathcal{F}^{-1}[\hat{\boldsymbol{u}}]$ is the inverse Fourier transform of $\hat{\boldsymbol{u}}$ and $\Re$ is the real part. As stated in Mansour and Wray[39], although rather unrealistic as initial conditions, the spectrum evolves toward the expected shape at a later time. The initial value for the Reynolds number based on the Taylor microscale λ, i.e. :

$$\mathrm{Re}_\lambda = E\sqrt{\frac{20}{3\,\nu\epsilon}}$$

($\epsilon = -\partial E/\partial t$ being the dissipation rate) is around 1500, whereas it drops to 500 at the final time $tU/L = 5$. The simulations were carried out with three different discretizations, namely 64^3, 128^3 and 256^3 particles initially arranged on a Cartesian lattice.

The two coarsest grids were also used to compute the turbulent decay without the proposed LES filtering, in order to highlight its effect. The results are shown in figure 9 for both simulations, along with the initial spectra. It can be clearly seen that the spectrum evolves towards the expected shape (i.e. with an inertial range with slope $-5/3$) only for the simulations with LES filtering, the direct simulations being too coarse to capture the proper energy cascade.

The comparison of the simulations for the three particle resolutions is shown in figure 10, where it can be clearly seen that, as expected, the amount of resolved kinetic energy increases with the resolution, because the reduced particle spacing is driving the simulation toward a resolved direct simulation.
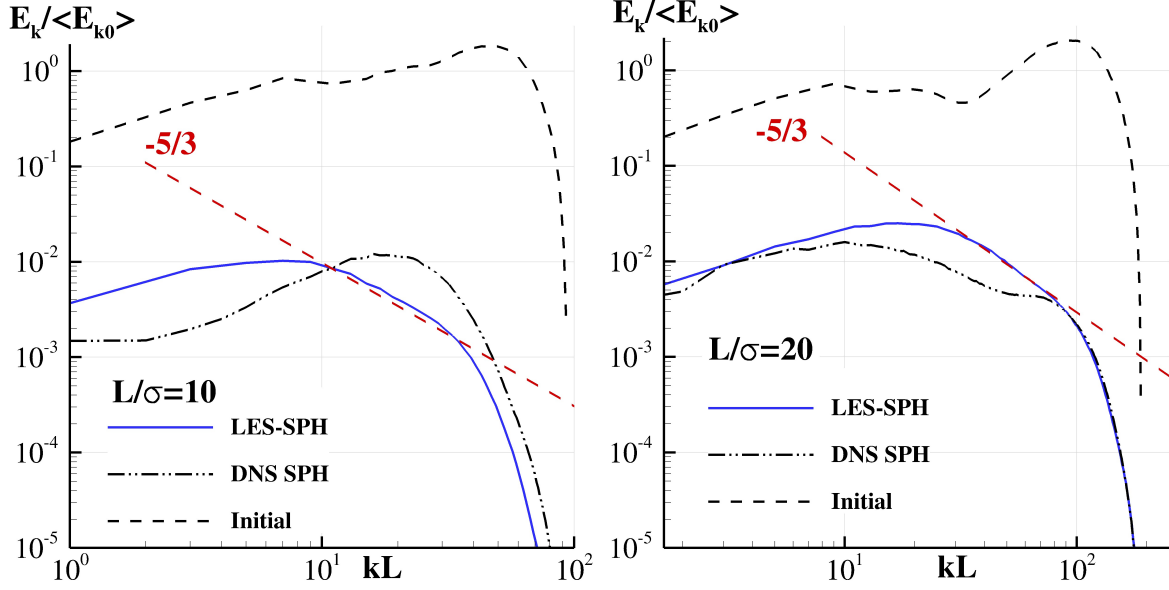
FIG. 9. Three-dimensional homogeneous turbulence decay. Comparison between DNS-SPH and LES-SPH simulations at $tU/L = 5$. Left: particle resolution 64^3. Right: particle resolution 128^3. Initial spectra are also shown. The spectra are scaled with the average initial kinetic energy $< E_{k0} >$.
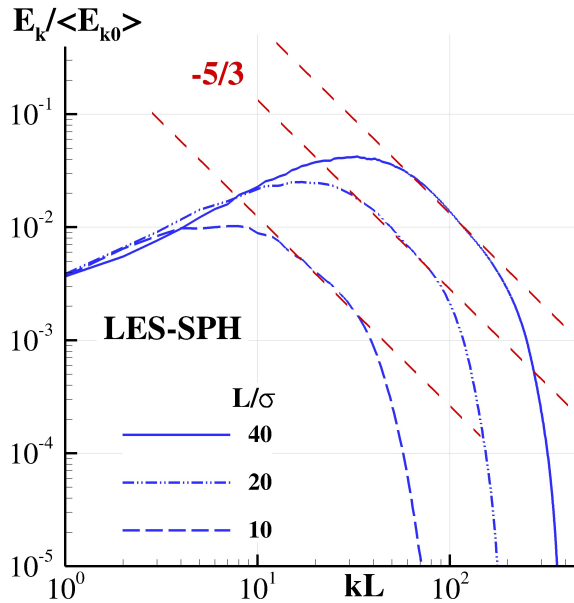

FIG. 10. Three-dimensional homogeneous turbulence decay. Comparison among different resolutions at $tU/L = 5$. The spectra are scaled with the average initial kinetic energy $< E_{k0} >$.

The computed vorticity fields are reported in figure 11 for the simulation with 128^3 particles with and without the LES modeling. It can be seen that the under-resolved direct

simulation causes the persistence of high-frequency components that, on the contrary, are quickly damped when the LES filter is applied.
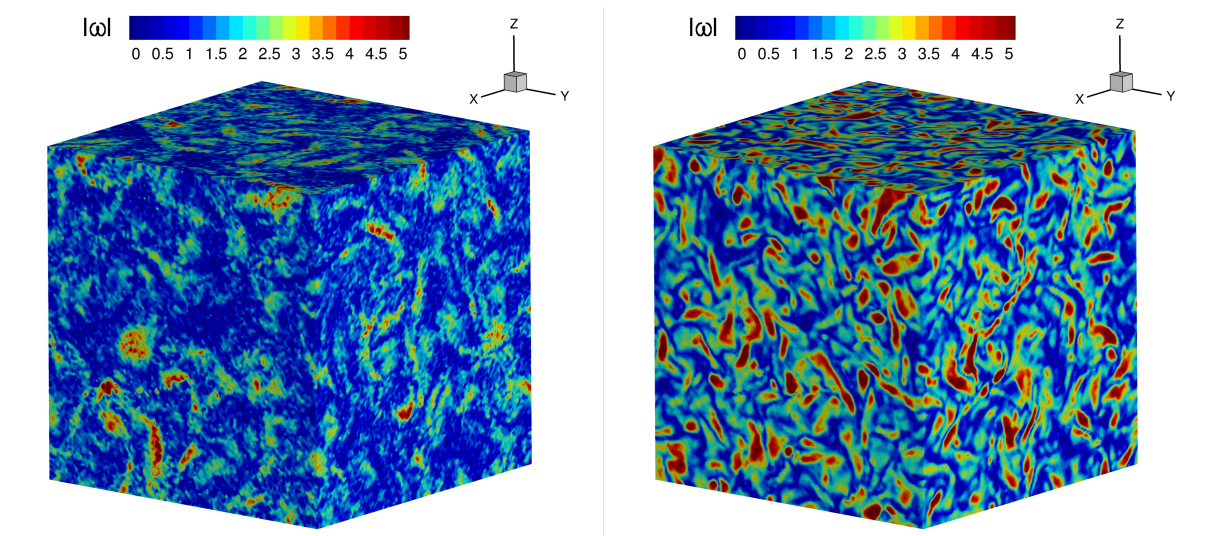

FIG. 11. Three-dimensional homogeneous turbulence decay at $\mathrm{Re}_\lambda = 500$. Comparison between the intensities of the vorticity fields for DNS-SPH (left) and LES-SPH simulations (right) using a particle resolution equal to 128^3.

VII. CONCLUSIONS

In the present paper, a general LES-SPH model is defined. First, Large Eddy Simulation is reformulated in a Lagrangian context by filtering all the variables in both time and space; this procedure allows maintaining the Lagrangian structure of the Navier–Stokes equations in term of material derivatives computed on particles that move with the filtered velocity.

The Lagrangian formulation of LES is then used to re–interpret the SPH approximation of differential operators as a specific model based on the decomposition of the LES filter into a spatial and time filter. The derived equations represent a general LES-SPH scheme and contain terms that in part come from LES filtering and in part derive from SPH kernels. The last ones lead to additional terms (with respect to LES filtering) that contain fluctuations in space, requiring adequate modeling. Finally, a closure of the LES-SPH scheme is proposed; the model is then implemented in a numerical code, and some numerical simulations are reported for free decay of two– and three–dimensional homogeneous and isotropic turbulence. The obtained results prove that the expected characteristics of the flow evolution are well

captured by SPH simulations with relatively coarse particle discretization, if the correct LES modeling is included.

It is to be underlined that no rigorous calibration of the coefficients that appear in the model was performed, because the main goal of the paper was to outline a correct LES filtering procedure in the SPH framework.

Future studies will be devoted to an in-depth analysis of the additional terms of the LES-SPH scheme and to the extension of the proposed model in finite domains (e.g., in the presence of walls and/or fluid-fluid interfaces). This remains a major issue in LES-SPH simulations of turbulence (see, for example, Mayrhofer et al.[19]).

ACKNOWLEDGEMENTS

Appendix A: Large Eddy Simulation in a Lagrangian framework: details of computation

We first focus on the derivation of the filtered momentum equation and consider the Lagrangian derivative of $\tilde{\boldsymbol{u}}$. Using the definition in (5), we obtain:

$$
\begin{aligned}
\frac{d\tilde{\boldsymbol{u}}}{dt} &= \frac{d}{dt} \int_{\mathbb{R}^3} \int_{-\infty}^{+\infty} \phi\left(\tilde{\boldsymbol{x}}_p - \boldsymbol{y}, t - \tau\right) \boldsymbol{u}\left(\boldsymbol{y}, \tau\right) d\tau \, dV_y \\
&= \int_{\mathbb{R}^3} \int_{-\infty}^{+\infty} \frac{d}{dt} \phi\left(\tilde{\boldsymbol{x}}_p - \boldsymbol{y}, t - \tau\right) \boldsymbol{u}\left(\boldsymbol{y}, \tau\right) d\tau \, dV_y \\
&= \int_{\mathbb{R}^3} \int_{-\infty}^{+\infty} \left[\frac{\partial \phi\left(\tilde{\boldsymbol{x}}_p - \boldsymbol{y}, t - \tau\right)}{\partial t} + \frac{d\tilde{\boldsymbol{x}}_p}{dt} \cdot \nabla_x \phi\left(\tilde{\boldsymbol{x}}_p - \boldsymbol{y}, t - \tau\right) \right] \boldsymbol{u}\left(\boldsymbol{y}, \tau\right) d\tau \, dV_y \\
&= \int_{\mathbb{R}^3} \int_{-\infty}^{+\infty} \left[\frac{\partial \phi\left(\tilde{\boldsymbol{x}}_p - \boldsymbol{y}, t - \tau\right)}{\partial t} + \tilde{\boldsymbol{u}}\left(\tilde{\boldsymbol{x}}_p, t\right) \cdot \nabla_x \phi\left(\tilde{\boldsymbol{x}}_p - \boldsymbol{y}, t - \tau\right) \right] \boldsymbol{u}\left(\boldsymbol{y}, \tau\right) d\tau \, dV_y \,. \text{(A1)}
\end{aligned}
$$

Since the filter has a compact support, we can integrate by parts and drop the contributions of the boundary integrals. Specifically, we can write:

$$
\begin{aligned}
&\int_{\mathbb{R}^3} \int_{-\infty}^{+\infty} \frac{\partial \phi\left(\tilde{\boldsymbol{x}}_p - \boldsymbol{y}, t - \tau\right)}{\partial t} \boldsymbol{u}\left(\boldsymbol{y}, \tau\right) d\tau \, dV_y \\
&= -\int_{\mathbb{R}^3} \int_{-\infty}^{+\infty} \frac{\partial \phi\left(\tilde{\boldsymbol{x}}_p - \boldsymbol{y}, t - \tau\right)}{\partial \tau} \boldsymbol{u}\left(\boldsymbol{y}, \tau\right) d\tau \, dV_y \\
&= \int_{\mathbb{R}^3} \int_{-\infty}^{+\infty} \left[-\frac{\partial \left[\phi\left(\tilde{\boldsymbol{x}}_p - \boldsymbol{y}, t - \tau\right) \boldsymbol{u}\left(\boldsymbol{y}, \tau\right)\right]}{\partial \tau} + \phi\left(\tilde{\boldsymbol{x}}_p - \boldsymbol{y}, t - \tau\right) \frac{\partial \boldsymbol{u}\left(\boldsymbol{y}, \tau\right)}{\partial \tau} \right] d\tau \, dV_y \\
&= \int_{\mathbb{R}^3} \int_{-\infty}^{+\infty} \phi\left(\tilde{\boldsymbol{x}}_p - \boldsymbol{y}, t - \tau\right) \frac{\partial \boldsymbol{u}\left(\boldsymbol{y}, \tau\right)}{\partial \tau} d\tau \, dV_y \,. \tag{A2}
\end{aligned}
$$

Similarly, it follows:

$$
\begin{aligned}
&\int_{\mathbb{R}^3} \int_{-\infty}^{+\infty} \left[\tilde{\boldsymbol{u}}\left(\tilde{\boldsymbol{x}}_p, t\right) \cdot \nabla_x \phi\left(\tilde{\boldsymbol{x}}_p - \boldsymbol{y}, t - \tau\right) \right] \boldsymbol{u}\left(\boldsymbol{y}, \tau\right) d\tau \, dV_y \\
&= \int_{\mathbb{R}^3} \int_{-\infty}^{+\infty} \left[-\tilde{\boldsymbol{u}}\left(\tilde{\boldsymbol{x}}_p, t\right) \cdot \nabla_y \phi\left(\tilde{\boldsymbol{x}}_p - \boldsymbol{y}, t - \tau\right) \right] \boldsymbol{u}\left(\boldsymbol{y}, \tau\right) d\tau \, dV_y \\
&= \int_{\mathbb{R}^3} \int_{-\infty}^{+\infty} \left\{ \tilde{\boldsymbol{u}}(\tilde{\boldsymbol{x}}_p, t) \cdot \nabla_y \left[-\phi(\tilde{\boldsymbol{x}}_p - \boldsymbol{y}, t - \tau) \, \boldsymbol{u}(\boldsymbol{y}, \tau) \right] + \phi(\tilde{\boldsymbol{x}}_p - \boldsymbol{y}, t - \tau) \, \tilde{\boldsymbol{u}}(\tilde{\boldsymbol{x}}_p, t) \cdot \nabla_y \boldsymbol{u}(\boldsymbol{y}, \tau) \right\} d\tau \, dV_y \\
&= \int_{\mathbb{R}^3} \int_{-\infty}^{+\infty} \phi\left(\tilde{\boldsymbol{x}}_p - \boldsymbol{y}, t - \tau\right) \tilde{\boldsymbol{u}}\left(\tilde{\boldsymbol{x}}_p, t\right) \cdot \nabla_y \boldsymbol{u}\left(\boldsymbol{y}, \tau\right) d\tau \, dV_y \,. \tag{A3}
\end{aligned}
$$

Therefore, summing up the two terms, we find:

$$
\begin{aligned}
\frac{d\tilde{\boldsymbol{u}}}{dt} &= \int_{\mathbb{R}^3} \int_{-\infty}^{+\infty} \frac{d}{dt} \phi\left(\tilde{\boldsymbol{x}}_p - \boldsymbol{y}, t - \tau\right) \boldsymbol{u}\left(\boldsymbol{y}, \tau\right) d\tau \, dV_y \\
&= \int_{\mathbb{R}^3} \int_{-\infty}^{+\infty} \phi\left(\tilde{\boldsymbol{x}}_p - \boldsymbol{y}, t - \tau\right) \left[\frac{\partial \boldsymbol{u}\left(\boldsymbol{y}, \tau\right)}{\partial \tau} + \tilde{\boldsymbol{u}}\left(\tilde{\boldsymbol{x}}_p, t\right) \cdot \nabla_y \boldsymbol{u}\left(\boldsymbol{y}, \tau\right) \right] d\tau \, dV_y \tag{A4}
\end{aligned}
$$

The integrand can be rewritten as follows:

$$\frac{\partial \boldsymbol{u}\left(\boldsymbol{y},\tau\right)}{\partial \tau} + \tilde{\boldsymbol{u}}\left(\tilde{\boldsymbol{x}}_p, t\right) \cdot \nabla_y \boldsymbol{u}\left(\boldsymbol{y},\tau\right)$$

$$= \frac{\partial \boldsymbol{u}\left(\boldsymbol{y},\tau\right)}{\partial \tau} + \left[\tilde{\boldsymbol{u}}\left(\tilde{\boldsymbol{x}}_p, t\right) - \boldsymbol{u}\left(\boldsymbol{y},\tau\right) + \boldsymbol{u}\left(\boldsymbol{y},\tau\right)\right] \cdot \nabla_y \boldsymbol{u}\left(\boldsymbol{y},\tau\right)$$

$$= \frac{\partial \boldsymbol{u}\left(\boldsymbol{y},\tau\right)}{\partial \tau} + \boldsymbol{u}\left(\boldsymbol{y},\tau\right) \cdot \nabla_y \boldsymbol{u}\left(\boldsymbol{y},\tau\right) + \left[\tilde{\boldsymbol{u}}\left(\tilde{\boldsymbol{x}}_p, t\right) - \boldsymbol{u}\left(\boldsymbol{y},\tau\right)\right] \cdot \nabla_y \boldsymbol{u}\left(\boldsymbol{y},\tau\right)$$

$$= \frac{d\boldsymbol{u}\left(\boldsymbol{y},\tau\right)}{d\tau} + \left[\tilde{\boldsymbol{u}}\left(\tilde{\boldsymbol{x}}_p, t\right) - \boldsymbol{u}\left(\boldsymbol{y},\tau\right)\right] \cdot \nabla_y \boldsymbol{u}\left(\boldsymbol{y},\tau\right)$$

$$= -\frac{1}{\rho}\nabla_y p + \nu \Delta_y \boldsymbol{u}\left(\boldsymbol{y},\tau\right) + (\nu + \lambda')\nabla_y \left(\nabla_y \cdot \boldsymbol{u}\left(\boldsymbol{y},\tau\right)\right) + \left[\tilde{\boldsymbol{u}}\left(\tilde{\boldsymbol{x}}_p, t\right) - \boldsymbol{u}\left(\boldsymbol{y},\tau\right)\right] \cdot \nabla_y \boldsymbol{u}\left(\boldsymbol{y},\tau\right)$$

Let us focus on the first term of the above expression. First, we introduce the variable $G(\rho)$:

$$G(\rho) = \int^{\rho} \frac{1}{s} \frac{dF}{ds}\, ds \quad \Rightarrow \quad \frac{1}{\rho}\nabla_y p = \nabla_y G(\rho) . \tag{A5}$$

Then, integrating by parts, we obtain:

$$-\int_{\mathbb{R}^3}\int_{-\infty}^{+\infty} \phi\left(\tilde{\boldsymbol{x}}_p - \boldsymbol{y}, t - \tau\right)\frac{1}{\rho}\nabla_y p\, d\tau\, dV_y$$

$$= -\int_{\mathbb{R}^3}\int_{-\infty}^{+\infty} \phi\left(\tilde{\boldsymbol{x}}_p - \boldsymbol{y}, t - \tau\right)\nabla_y G(\rho)\, d\tau\, dV_y$$

$$= \int_{\mathbb{R}^3}\int_{-\infty}^{+\infty} \nabla_y\phi\left(\tilde{\boldsymbol{x}}_p - \boldsymbol{y}, t - \tau\right) G(\rho)\, d\tau\, dV_y$$

$$= -\int_{\mathbb{R}^3}\int_{-\infty}^{+\infty} \nabla_x\phi\left(\tilde{\boldsymbol{x}}_p - \boldsymbol{y}, t - \tau\right) G(\rho)\, d\tau\, dV_y = -\nabla_x\widetilde{G(\rho)} . \tag{A6}$$

Since we work on the variable $\tilde{\rho}$, we rearrange the above result as follows:

$$-\nabla_x\widetilde{G(\rho)} = -\nabla_x G(\tilde{\rho}) - \nabla_x\left[\widetilde{G(\rho)} - G(\tilde{\rho})\right] = -\frac{1}{\tilde{\rho}}\nabla_x\tilde{p} - \nabla_x\left[\widetilde{G(\rho)} - G(\tilde{\rho})\right], \tag{A7}$$

where $\tilde{p}$ is given by (7). The remaining terms of the integral are rearranged by using the properties of the filter. We obtain:

$$\int_{\mathbb{R}^3}\int_{-\infty}^{+\infty} \phi\left(\tilde{\boldsymbol{x}}_p - \boldsymbol{y}, t - \tau\right)\Delta_y \boldsymbol{u}\left(\boldsymbol{y},\tau\right)\, d\tau\, dV_y = \Delta_x\tilde{\boldsymbol{u}}\left(\tilde{\boldsymbol{x}}_p, t\right) \tag{A8}$$

$$\int_{\mathbb{R}^3}\int_{-\infty}^{+\infty} \phi\left(\tilde{\boldsymbol{x}}_p - \boldsymbol{y}, t - \tau\right)\nabla_y\left(\nabla_y \cdot \boldsymbol{u}\left(\boldsymbol{y},\tau\right)\right)\, d\tau\, dV_y = \nabla_x\left(\nabla_x \cdot \tilde{\boldsymbol{u}}\left(\tilde{\boldsymbol{x}}_p, t\right)\right) \tag{A9}$$

The last integrand term deserves a special attention. First, we write:

$$\int_{\mathbb{R}^3} \int_{-\infty}^{+\infty} \phi\left(\tilde{\boldsymbol{x}}_p - \boldsymbol{y}, t - \tau\right) \left[\left[\tilde{\boldsymbol{u}}\left(\tilde{\boldsymbol{x}}_p, t\right) - \boldsymbol{u}\left(\boldsymbol{y}, \tau\right)\right] \cdot \nabla_y \boldsymbol{u}\left(\boldsymbol{y}, \tau\right)\right] d\tau \, dV_y$$

$$= \int_{\mathbb{R}^3} \int_{-\infty}^{+\infty} \phi\left(\tilde{\boldsymbol{x}}_p - \boldsymbol{y}, t - \tau\right) \nabla_y \left[\left[\tilde{\boldsymbol{u}}\left(\tilde{\boldsymbol{x}}_p, t\right) - \boldsymbol{u}\left(\boldsymbol{y}, \tau\right)\right] \otimes \boldsymbol{u}\left(\boldsymbol{y}, \tau\right)\right] d\tau \, dV_y$$

$$+ \int_{\mathbb{R}^3} \int_{-\infty}^{+\infty} \phi\left(\tilde{\boldsymbol{x}}_p - \boldsymbol{y}, t - \tau\right) \left[\nabla_y \cdot \boldsymbol{u}\left(\boldsymbol{y}, \tau\right)\right] \boldsymbol{u}\left(\boldsymbol{y}, \tau\right) d\tau \, dV_y \qquad (A10)$$

Then, using again the properties of the filter, we obtain:

$$\int_{\mathbb{R}^3} \int_{-\infty}^{+\infty} \phi\left(\tilde{\boldsymbol{x}}_p - \boldsymbol{y}, t - \tau\right) \left[\left[\tilde{\boldsymbol{u}}\left(\tilde{\boldsymbol{x}}_p, t\right) - \boldsymbol{u}\left(\boldsymbol{y}, \tau\right)\right] \cdot \nabla_y \boldsymbol{u}\left(\boldsymbol{y}, \tau\right)\right] d\tau \, dV_y = \nabla_x \cdot \mathbb{T}_\ell + \widetilde{\boldsymbol{u} \, \nabla \cdot \boldsymbol{u}},$$

where the tensor $\mathbb{T}_\ell$ is given by

$$\boxed{\mathbb{T}_\ell = \int_{\mathbb{R}^3} \int_{-\infty}^{+\infty} \phi\left(\tilde{\boldsymbol{x}}_p - \boldsymbol{y}, t - \tau\right) \left[\tilde{\boldsymbol{u}}\left(\tilde{\boldsymbol{x}}_p, t\right) - \boldsymbol{u}\left(\boldsymbol{y}, \tau\right)\right] \otimes \boldsymbol{u}\left(\boldsymbol{y}, \tau\right) d\tau \, dV_y = \tilde{\boldsymbol{u}} \otimes \tilde{\boldsymbol{u}} - \widetilde{\boldsymbol{u} \otimes \boldsymbol{u}}}.$$

Summarizing, the filtered momentum equation reads:

$$\boxed{\frac{d\tilde{\boldsymbol{u}}}{dt} = -\frac{\nabla \tilde{p}}{\tilde{\rho}} + \nu \Delta \tilde{\boldsymbol{u}} + (\lambda' + \nu) \nabla\left(\nabla \cdot \tilde{\boldsymbol{u}}\right) - \nabla\left[\widetilde{G(\rho)} - G(\tilde{\rho})\right] + \nabla \cdot \mathbb{T}_\ell + \widetilde{\boldsymbol{u} \, \nabla \cdot \boldsymbol{u}}.} \quad (A11)$$

As to the continuity equation, the filtering procedure leads to the following result:

$$\boxed{\frac{d\tilde{\rho}}{dt} = -\tilde{\rho} \, \nabla \cdot \tilde{\boldsymbol{u}} + \nabla \cdot \left[\tilde{\rho}\tilde{\boldsymbol{u}} - \widetilde{\rho \boldsymbol{u}}\right].} \qquad (A12)$$

1. Non commutability of the spatial and time filters

Here we provide an estimate of the difference between $\langle \overline{f} \rangle$ and $\overline{\langle f \rangle}$. Let us consider the following expansions:

$$\tilde{\boldsymbol{x}}_p(t) = \tilde{\boldsymbol{x}}_p(\tau) + \tilde{\boldsymbol{u}}(t)\left(t - \tau\right) + \mathcal{O}\left(|t - \tau|^2\right), \qquad (A13)$$

$$W\left(\tilde{\boldsymbol{x}}_p(t) - y\right) = W\left(\tilde{\boldsymbol{x}}_p(\tau) - y\right) + \nabla W\big|_{\tilde{\boldsymbol{x}}_p(t)} \cdot \tilde{\boldsymbol{u}}(t)\left(t - \tau\right) + \mathcal{O}\left(|t - \tau|^2\right). \quad (A14)$$

We multiply the latter equation for the time filter $\theta(t - \tau)$ and for a scalar field $f(\boldsymbol{y}, \tau)$, obtaining:

$$W\left(\tilde{\boldsymbol{x}}_p(t) - y\right)\theta(t - \tau)\,f(\boldsymbol{y}, \tau) =$$

$$W\left(\tilde{\boldsymbol{x}}_p(\tau) - y\right)\theta(t - \tau)\,f(\boldsymbol{y}, \tau)\,+\,\nabla W\big|_{\tilde{\boldsymbol{x}}_p(t)} \cdot \tilde{\boldsymbol{u}}(t)\,(t - \tau)\,\theta(t - \tau)\,f(\boldsymbol{y}, \tau)\,+\,\mathcal{O}\left(|\,t - \tau\,|^2\right) =$$

$$W\left(\tilde{\boldsymbol{x}}_p(\tau) - y\right)\theta(t - \tau)\,f(\boldsymbol{y}, \tau)\,+\,\nabla W\big|_{\tilde{\boldsymbol{x}}_p(t)} \cdot \tilde{\boldsymbol{u}}(t)\,(t - \tau)\,\theta(t - \tau)\,f(\boldsymbol{y}, t)\,+\,\mathcal{O}\left(|\,t - \tau\,|^2\right).$$

Integrating over $(\boldsymbol{y}, \tau) \in \mathbb{R}^3 \times \mathbb{R}$, we find:

$$\langle \overline{f} \rangle \,=\, \overline{\langle f \rangle}\,+\,\epsilon\,\gamma\,\tilde{\boldsymbol{u}} \cdot \langle \nabla f \rangle\,+\,\mathcal{O}(\epsilon^2)\,, \tag{A15}$$

where ϵ is a reference period of the compact support of $\theta(t - \tau)$ and

$$\int_{\mathbb{R}} (t - \tau)\,\theta(t - \tau)\,d\tau \,=\, \epsilon\,\gamma\,. \tag{A16}$$

If θ is even, then $\gamma = 0$ and the overall error is of order $\mathcal{O}(\epsilon^2)$.

REFERENCES

[1] A. Colagrossi and M. Landrini, "Numerical Simulation of Interfacial Flows by Smoothed Particle Hydrodynamics", *J. Comp. Phys.*, vol. 191, pp. 448–475, 2003.

[2] J. J. Monaghan, "Smoothed particle hydrodynamics," *Reports on Progress in Physics*, vol. 68, pp. 1703–1759, 2005.

[3] V. Springel, "Smoothed particle hydrodynamics in astrophysics", *Annual Review of Astronomy and Astrophysics*, vol. 48, pp. 391–430, 2010.

[4] D. Wilcox, *Turbulence modeling for CFD.* DCW industries La Canada, CA, 1998, vol. 2.

[5] D. Violeau and R. Issa, "Numerical modelling of complex turbulent free surface flows with the SPH Lagrangian method: an overview", *Int. J. Num. Meth. Fluids*, vol. 53(2), pp. 277–304, 2006.

[6] D. De Padova, M. Mossa, and S. Sibilla, "SPH numerical investigation of the velocity field and vorticity generation within a hydrofoil-induced spilling breaker", *Environmental Fluid Mechanics*, vol. 16, no. 1, pp. 267–287, 2016.

[7] A. Leroy, D. Violeau, M. Ferrand, and C. Kassiotis, "Unified semi-analytical wall boundary conditions for 2-D incompressible SPH", *J. Comput. Phys.*, vol. 261, pp. 106–129, 2014.

[8] M. Lesieur and O. Métais, "New trends in large-eddy simulations of turbulence", *Annual Review of Fluid Mechanics*, vol. 28, no. 1, pp. 45–82, 1996.

[9] U. Piomelli, "Large-eddy simulation: achievements and challenges", *Progress in Aerospace Sciences*, vol. 35, no. 4, pp. 335–362, 1999.

[10] C. Meneveau and J. Katz, "Scale-invariance and turbulence models for large-eddy simulation", *Annual Review of Fluid Mechanics*, vol. 32, no. 1, pp. 1–32, 2000.

[11] U. Piomelli and E. Balaras, "Wall-layer models for large-eddy simulations", *Annual review of fluid mechanics*, vol. 34, no. 1, pp. 349–374, 2002.

[12] P. R. Spalart, *Trends in turbulence treatments*. American Institute of Aeronautics and Astronautics, 2000.

[13] A. Colagrossi, M. Antuono, and D. Le Touzé, "Theoretical considerations on the free-surface role in the Smoothed-particle-hydrodynamics model", *Physical Review E*, vol. 79, no. 5, p. 056701, 2009.

[14] A. Colagrossi, M. Antuono, A. Souto-Iglesias, and D. Le Touzé, "Theoretical analysis and numerical verification of the consistency of viscous smoothed-particle-hydrodynamics formulations in simulating free-surface flows", *Physical Review E*, vol. 84, p. 026705, 2011.

[15] H. Gotoh, T. Shibahara, and T. Sakai, "Sub-particle-scale turbulence model for the MPS method - Lagrangian flow model for hydraulic engineering", *Advanced Methods for Computational Fluid Dynamics*, vol. 9, no. 4, pp. 339–347, 2001.

[16] D. Violeau, S. Piccon, and C. J.-P., "Two attempts of turbulence modelling in Smoothed Particle Hydrodynamics", in *Proceedings of the 8th International Symposium on Flow Modeling and Turbulence Measurements*, vol. 4. World Scientific, 2001, p. 6.

[17] E. Y. Lo and S. Shao, "Simulation of near-shore solitary wave mechanics by an incompressible SPH method", *Applied Ocean Research*, vol. 24, no. 5, pp. 275–286, 2002.

[18] R. Dalrymple and B. Rogers, "Numerical modeling of water waves with the SPH method", *Coastal Engineering*, vol. 53 (2-3), pp. 141–147, 2006.

[19] A. Mayrhofer, D. Laurence, B. Rogers, and D. Violeau, "DNS and LES of 3-D wall-bounded turbulence using Smoothed Particle Hydrodynamics", *Computers & Fluids*, vol. 115, pp. 86–97, 2015.

[20] J. Monaghan, "Simulating Free Surface Flows with SPH", *J. Comp. Phys.*, vol. 110, no. 2, pp. 39–406, 1994.

[21] S. Marrone, A. Colagrossi, A. Di Mascio, and D. Le Touzé, " Prediction of energy losses in water impacts using incompressible and weakly compressible models ", *Journal of Fluids and Structures*, vol. 54, pp. 802–822, 2015.

[22] M. Germano, U. Piomelli, P. Moin, and W. H. Cabot, "A dynamic subgrid-scale eddy viscosity model", *Physics of Fluids A: Fluid Dynamics (1989-1993)*, vol. 3, no. 7, pp. 1760–1765, 1991.

[23] P. Moin, K. Squires, W. Cabot, and S. Lee, "A dynamic subgrid-scale model for compressible turbulence and scalar transport", *Physics of Fluids A*, vol. 3, no. 11, pp. 2746–2757, 1991.

[24] D. Violeau and A. Leroy, "On the maximum time step in weakly compressible SPH", *Journal of Computational Physics*, vol. 256, pp. 388–415, 2014.

[25] W. Dehnen and H. Aly, "Improving convergence in smoothed particle hydrodynamics simulations without pairing instability", *Monthly Notices of the Royal Astronomical Society*, vol. 425, no. 2, pp. 1068–1082, 2012.

[26] A. Yoshizawa, "Statistical theory for compressible turbulent shear flows, with the application to subgrid modeling", *Physics of Fluids*, vol. 29, p. 2152, 1986.

[27] D. Molteni and A. Colagrossi, "A simple procedure to improve the pressure evaluation in hydrodynamic context using the SPH", *Computer Physics Communications*, vol. 180, pp. 861–872, 2009.

[28] D. Le Touzé, A. Colagrossi, G. Colicchio, and M. Greco, "A critical investigation of smoothed particle hydrodynamics applied to problems with free-surfaces", *International Journal for Numerical Methods in Fluids*, vol. 73, no. 7, pp. 660–691, 2013.

[29] J. P. Morris, P. J. Fox, and Y. Zhu, "Modeling Low Reynolds Number Incompressible Flows Using SPH", *Journal of Computational Physics*, vol. 136, pp. 214–226, 1997.

[30] T. Belytschko, Y. Krongauz, J. Dolbow, and C. Gerlach, "On the completeness of meshfree particle methods", *Int. J. Numer. Methods Engineering*, vol. 43, no. 5, pp. 785–819, Nov. 1998.

[31] A. Colagrossi, A. Souto-Iglesias, M. Antuono, and S. Marrone, "Smoothed-particle-hydrodynamics modeling of dissipation mechanisms in gravity waves", *Phys. Rev. E*, vol. 87, p. 023302, Feb 2013.

[32] A. Colagrossi, B. Bouscasse, M. Antuono, and S. Marrone, "Particle packing algorithm for SPH schemes", *Computer Physics Communications*, vol. 183, no. 2, pp. 1641–1683, 2012.

[33] M. Antuono, B. Bouscasse, A. Colagrossi, and S. Marrone, "A measure of spatial disorder in particle methods", *Computer Physics Communications*, vol. 185, no. 10, pp. 2609–2621, 2014.

[34] Y. Shi, X. X. Zhu, M. Ellero, and N. A. Adams, "Analysis of interpolation schemes for the accurate estimation of energy spectrum in Lagrangian methods", *Computers & Fluids*, vol. 82, pp. 122–131, 2013.

[35] P. Tabeling, "Two-dimensional turbulence: a physicist approach", *Physics Reports*, vol. 362, no. 1, pp. 1–62, 2002.

[36] J. W. Swegle, D. L. Hicks, and S. W. Attaway, "Smoothed Particle Hydrodynamics Stability Analysis", *Journal of Computational Physics*, vol. 116, pp. 123–134, 1995.

[37] R. Kraichnan, "Inertial Ranges in Two-Dimensional Turbulence", *Physics of Fluids*, vol. 10, no. 7, pp. 1417–1423, 1967.

[38] M. Ellero, P. Español, and N. A. Adams, "Implicit atomistic viscosities in smoothed particle hydrodynamics", *Phys. Rev. E*, vol. 82, no. 4, p. 046702, Oct 2010.

[39] N. Mansour and A. Wray, "Decay of isotropic turbulence at low Reynolds number", *Physics of Fluids*, vol. 6, no. 2, pp. 808–814, 1994.

[40] M. Antuono, A. Colagrossi, S. Marrone, D. Molteni, "Free-surface flows solved by means of SPH schemes with numerical diffusive terms", *Comp. Phys. Comm.*, vol. 181, pp. 532–549, 2010.

[41] , GA. Blaisdell, NN. Mansour, WC. Reynolds, "Compressibility effects on the growth and structure of homogeneous turbulent shear flow", *Journal of Fluid Mechanics*, vol. 256, pp. 443–485, 1993.

[42] T. Passot, A. Pouquet. "Numerical simulation of compressible homogeneous flows in the turbulent regime", *Journal of Fluid Mechanics*, vol. 181, pp. 441–466, 1987.

[43] J. Suh, S.H. Frankel, L. Mongeau, M.W. Plesniak, "Compressible large eddy simulations of wall-bounded turbulent flows using a semi-implicit numerical scheme for low Mach number aeroacoustics", *Journal of Computational Physics*, vol. 215(2), pp. 526–551, 2006.